Supplementary Information for

Dynamic and static excimer: a versatile platform for single component white light emission and chelation-enhanced fluorescence

Virendra Kumar, Bahadur Sk, Subhankar Kundu and Abhijit Patra*

Department of Chemistry, Indian Institute of Science Education and Research Bhopal, Bhopal-462066, Fax: +91 (0)755 409 2392; Tel: +91 (0)755 669 1337

E-mail: abhijit@iiserb.ac.in

I. Materials and methods

(a) Chemicals:

All chemicals were used as received unless stated otherwise. 1-Pyrenecarboxaldehyde (99%), hydrazine hydrate (99%), guanidinium chloride (99%), coumarin-102 (99%) and poly(methyl methacrylate) (M_w = ~ 12000 Da) were received from Sigma-Aldrich. All the spectroscopic grade solvents [ethyl acetate (EA), acetonitrile (ACN), dimethyl sulfoxide (DMSO), methanol (MeOH), ethanol (EtOH), tetrahydrofuran (THF), dioxane (DIO), chloroform (CH) and dichloromethane (DCM)] were received from Spectrochem, India. Dichloromethane and chloroform were dried using calcium hydride and calcium chloride, respectively and subsequently distilled. Tetrahydrofuran was dried refluxing with sodium over benzophenone and distilled under nitrogen.

(b) Instrumentation:

NMR Spectroscopy:

^{1}H and ^{13}C-NMR spectra were recorded on Bruker Avance III 500 MHz NMR spectrometer and the chemical shifts (δ) are reported in parts per million (ppm) using residual solvent signals as internal standards.

FTIR Spectroscopy:

Fourier-transform infrared (FTIR) spectroscopic measurements were carried out on Perkin Elmer spectrophotometer. Ten scans were signal-averaged, with a resolution of 4 cm^{-1} at room temperature. KBr pellet was used for the measurements.

Matrix-Assisted Laser Desorption Ionization (MALDI-ToF):

Matrix-assisted laser desorption ionization time of flight mass spectrometry was performed with Bruker Daltonics UltrafleXtreme, using software flex Control version 3.4.

Steady-state absorption spectroscopy:

The UV-Vis absorption spectra were recorded on a Cary 100 spectrophotometer.

Steady-state fluorescence spectroscopy:

Steady-state fluorescence measurements were carried out on Jobin Yvon Horiba Model Fluorolog-3-21. All the fluorescence spectra were corrected with respect to the excitation light intensity and photomultiplier tube (PMT) response using the correction files available with Horiba software. The optical density of the samples was maintained low enough to avoid any inner filter effect.

Time-resolved fluorescence Spectroscopy:

Time-resolved fluorescence measurements were carried out using time-correlated single photon counting (TCSPC) spectrometer (Delta Flex-01-DD/HORIBA). Delta diode laser 408 nm were used as excitation source. Picosecond photon detection module with photomultiplier tube was used as a detector. The instrument response function was recorded by using an aqueous solution of Ludox. Decay curves were analyzed by nonlinear least-squares iteration using IBH DAS6 (version 6.8) decay analysis software. The quality of the fitting was assessed by the fitting parameters (χ^2) as well as the visual inspection of the residuals.

Electrochemical measurements:

Electrochemical measurements were performed using CH instrument. Glassy carbon, $Ag/AgNO_3$ (1 M $AgNO_3$) electrode and Pt wire were used respectively, as a working, reference and counter electrode in a three-electrode cell. All the measurements were done in dichloromethane solution with 0.1 M tetrabutylammonium hexafluorophosphate as supporting electrolyte. All the spectra were recorded at a scan rate of 100 mV/s at ambient temperature (25 ± 1 °C) under a nitrogen atmosphere.

Field emission scanning electron microscopy (FESEM):

Morphology of the aggregates was examined using Carl Zeiss (Ultraplus) field emission scanning electron microscope. The accelerating voltage of 5 kV and 20 kV were used. Samples for FESEM were prepared by drop casting on the aluminium stub using the adhesive carbon tape. All samples were coated with a thin layer of sputtered gold before imaging.

Differential scanning calorimetry (DSC):

The DSC analysis was carried out using Perkin Elmer instrument (DSC 6000) with software version: 11.0.0.0449. Instrument was calibrated with indium and zinc prior to the experiment.

Thermogravimetric analysis (TGA):

Thermogravimetric analysis was carried out in Perkin Elmer (TGA-4000) instrument with software version 11.0.0.0449. Sample was heated at a rate of 10 °C/min under nitrogen atmosphere.

II. Photophysical background of excimer formation

The term 'excimer' was first introduced by Stevens and Hutton in 1960 to explain the nature of an excited state dimer. According to them, excimer is an excited state dimer which is associated in an excited electronic state and dissociated in the ground electronic state. This definition is mostly valid for an intermolecular excimer (in a fluid medium) where the formation of the excimer is governed through intermolecular forces between an excited state and a ground state monomer. But this concept is quite unfitted for some particular systems where the monomeric units are in the constrained environment or rigid media. In such cases, the excimer formation found to be happening due to the intramolecular interactions between the monomeric units rather the intermolecular interactions. In view of such observation, in 1975, Birks proposed a revised definition of excimer as 'a dimer which is associated in an excited electronic state and which is dissociative (i.e., would dissociate in the absence of external restraints) in its ground electronic state'.[1] This definition suggests the two different ways of the formation of excimer. In the first case, the molecular photoassociation is achieved through the diffusion of a photoexcited monomer with a ground state monomer. This type of excimer is well known as dynamic excimer. Hence, the lifetime of the excited state monomer should be high enough to have a successful collision.[2,3] On the other hand, the rigid environment and some intramolecular interactions mostly favor the formation of ground state dimer, which is further photoexcited to give the static excimer.[2-4] The ground state of the static dimer is much more stabilized as compared to the dynamic counterpart due to the presence of some weak interactions (π-π, hydrophobic, etc.) between two monomeric units. On the other hand, the higher overlapping possibility of two molecular components makes the dynamic excimer more stable in the excited state. A broad, structureless and red-shifted fluorescence emission band was observed in case of excimer as compared to that of the monomer emission. The occurrence of static and dynamic nature of the excimer can be proved through the excitation spectra and time-dependent excimer emission profile. The excitation spectrum monitored at excimer emission is found to be broadened and red-shifted compared to that obtained at monomer emission in the case of static excimer. Whereas, the excitation spectra recorded at monomer and excimer emission are found to be similar for dynamic excimer.[4,5]

III. Design strategy

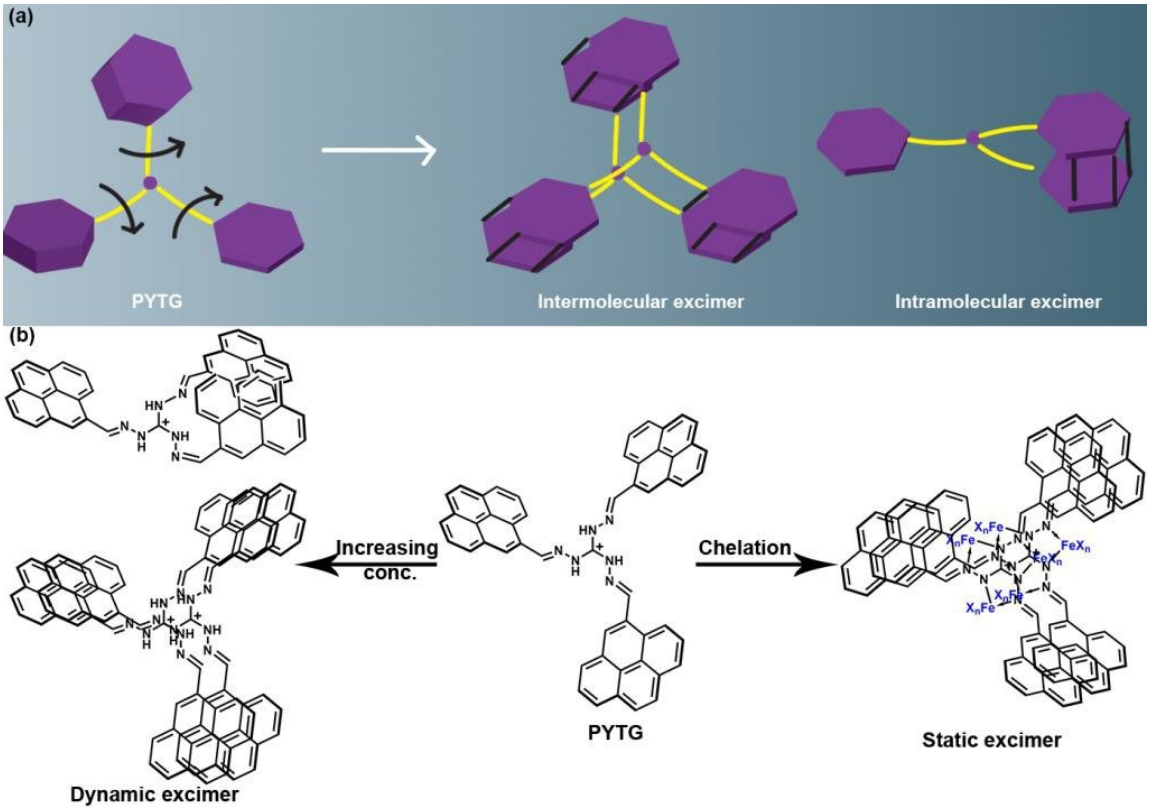

Scheme S1 Schematic illustration demonstrating the design strategy of the probe, PYTG, including the physical concept behind (a) inter and intramolecular, (b) dynamic and static excimer.

The in-depth understanding of excimer formation in functional materials is a fundamental importance to address in view of their profound utility in photophysical, biological and analytical applications.[6-11] Hence, we thought to develop a functional fluorescent material which can be used for the understanding of excimer formation and monitoring the stimuli responsive emission behavior as well as the detection of some essential elements. Pyrene was chosen as a component due to its dual emissive behavior consisting of both monomer and excimer emission.[2,3,12] Though native pyrene is well explored for the excimer formation; it is a challenge to differentiate between the static and dynamic excimer.

We thought to incorporate the pyrene moiety with another functional core. In this context, triaminoguanidinium chloride was chosen as the C_3-symmetric functional core for the accommodation of three pyrene rings through a simple one-step Schiff base condensation reaction. Though the triaminoguanidinium unit is C_3-symmetric, the tripodal architecture of the Schiff base product (PYTG), makes it nonplanar through the flexible imine connectors. These flexible

connectors with multiple pyrene units in PYTG are helpful to form facile excimer both through intra and intermolecular interactions which are not solely possible in rigid C_2-symmetric molecules (Scheme S1a). Additionally, the importance of C_3-symmetry in our system is the presence of several coordination sites. Triaminoguanidinium with bulky pyrene units create pockets or coordination sites for specific external ions (size may play a role along with electronic factors). Hence, the C_3-symmetry helps to form three specific coordination sites for ions to bind leading to the formation of static excimer (Scheme S1b).[13] On the other hand, due to the presence of an extended conjugation between pyrene units and central carbocation through the imine linkages, broad and structureless bands are quite predictable for both the monomer and excimer emissions. These bands are anticipated to cover the whole visible region generating white light at a particular experimental condition. The design strategy reflects that PYTG can be utilized as a versatile platform for understanding the excimer formation as well as detection of different types of essential ions along with the generation of white light emission.

IV. Synthesis and characterization

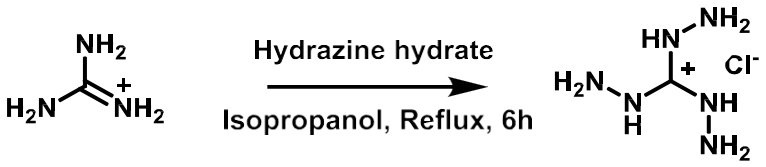

Scheme S2 Synthetic scheme of triaminoguanidinium chloride.

In a typical synthetic procedure, guanidinium chloride (1 mmol) was taken in 30 mL of isopropanol in a 100 mL round bottom flask. 50-60% hydrazine hydrate (4.5 mmol) was added to the above solution and was refluxed for 6 h. After the reaction, the precipitate was filtered and was washed with 50 mL of isopropanol to obtain triaminoguanidinium chloride (Scheme S2, yield: 97 %).

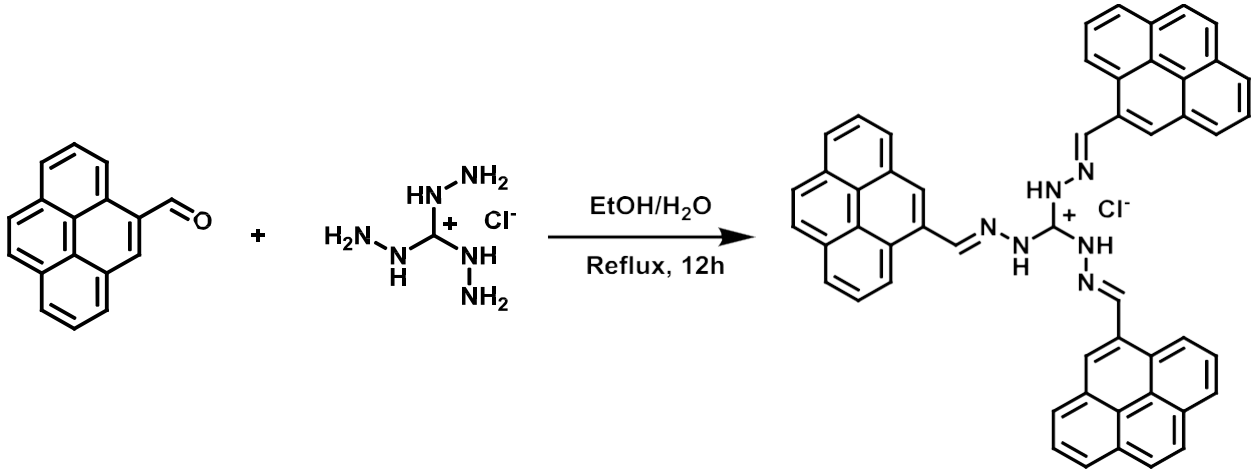

Scheme S3 Synthetic scheme of Schiff base condensation product between pyrene-1-carboxaldehyde and triaminoguanidinium chloride (PYTG).

Synthesis of pyrene-1-carboxaldehyde- triaminoguanidinium adduct (PYTG):

PYTG was synthezised by a one-step Schiff base condensation reaction (Scheme S3). In the typical procedure, triaminoguanidinium chloride (50 mg, 0.33 mmol) was dissolved in 10 mL ethanol/H_2O in a 100 mL round-bottomed flask. Then, pyrene-1-carboxaldehyde (230 mg, 1.0 mmol) was added with vigorous stirring and was refluxed for 12 h at 85°C temperature. The resulting precipitate was filtered and washed 3 times with ether. After drying under reduced pressure, PYTG was obtained as a light-yellow solid (yield: 85%). The molecular structure and purity of PYTG were established through ^{1}H NMR, ^{13}C NMR, and HRMS analysis (Fig S41-S43).

^{1}H NMR: (500 MHz, DMSO-d_6) δ_H (ppm): 12.52 (s, 3H), 10.08 (s, 3H), 9.19 (d, J = 8.1 Hz, 3H), 8.60 (d, J = 9.4 Hz, 3H), 8.45 (d, J = 8.2 Hz, 3H), 8.36 (dd, 9H), 8.27 – 8.18 (m, 6H), 8.13 (t, J = 7.5 Hz, 3H).

^{13}C NMR: (126 MHz, DMSO) δ (ppm): 149.61, 148.81, 132.96, 130.98, 130.31, 129.85, 129.15, 128.88, 127.44, 126.88, 126.71, 126.25, 125.80, 125.46, 124.79, 124.07, 123.84, 121.83.

HRMS (ESI): *m/z* calculated for $[PYTG]^+$ is 741.277 and found 741.2720.

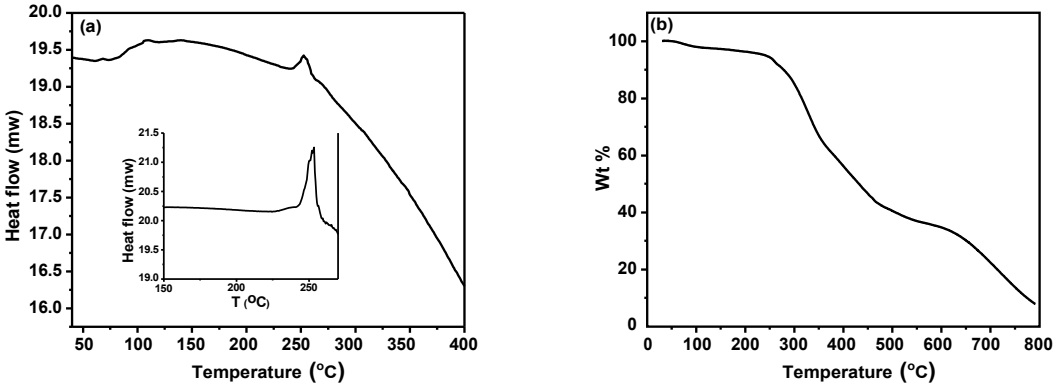

Fig. S1 (a) Differential scanning calorimetry (DSC) and (b) thermogravimetric analysis (TGA) of PYTG.

V. Spectroscopic Investigations

(a) Absorption, fluorescence emission and excitation measurements:

The spectroscopic features of PYTG were investigated in comparison with pyrene. The absorption and emission behavior of pyrene were monitored in chloroform with 5 μM concentration. The highly structured bands were observed for both the absorption and emission in case of pyrene due to its rigid and highly conjugated structure (Fig. S2). No significant excimer peak was noticed as compared to the monomer emission even at 5 μM concentration.

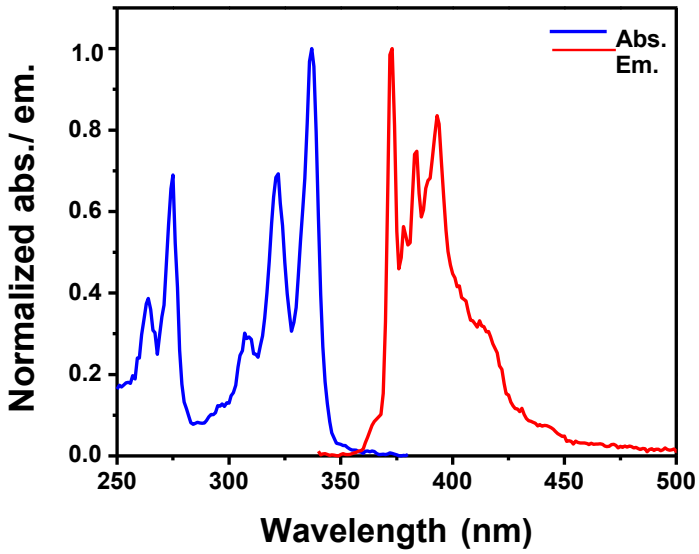

Fig. S2 Normalized absorption and emission (λ_{exc} = 330 nm) spectra of pyrene (5 μM) in $CHCl_3$.

The basic photophysical studies of PYTG were carried out in $CHCl_3$ with 0.5 μM concentration. A broad absorption band with two humps at nearly 390 and 410 nm were observed (main text, Fig. 1a), which is significantly red-shifted as compared to that of the structured absorption bands of pristine pyrene (230 to 350 nm, Fig. S2). The red-shifted absorption of PYTG can be attributed to the π-π* transition of pyrene moiety which is mostly due to the extended delocalization of π-electrons from electron rich pyrene rings to that of the electron deficient carbon centre of triaminoguanidinium through the imine linkage. The photophysical behaviour of PYTG in solvents with a broad range of polarities (as per the empirical parameter of solvent polarity, normalized E_T^N values mentioned in parenthesis against each solvent) were investigated.[14] The solvents used for the spectroscopic investigation were the following: toluene (TL, 0.099), dioxane (DIO, 0.164), tetrahydrofuran (THF, 0.207), ethyl acetate (EA, 0.228), chloroform (CH, 0.259),

dichloromethane (DCM, 0.309), dimethyl sulfoxide (DMSO, 0.444), acetonitrile (ACN, 0.460),

ethanol (EtOH, 0.654), methanol (MeOH, 0.762). Fig. S3 depicts that the absorption and emission of PYTG is almost independent of solvent polarity. The ratio of monomer to excimer emission intensity with varying the solvent polarity (THF, DIO, CH and DCM as in these solvents PYTG is emissive) was also checked. It was noticed that with the increasing polarity of the solvents the emission intensity of the monomer to that of the excimer decreases (Fig. S4). This is may be due to the facile formation of excimer in polar solvents.[15] Fig. S5 reveals that the excitation spectra of the excimer is almost independent on the polarity of the solvents.

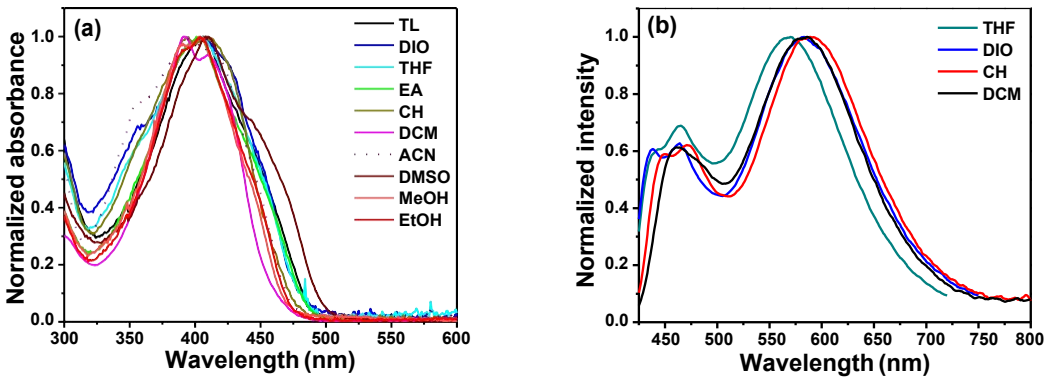

Fig. S3 Normalized (a) absorption and (b) emission spectra (λ_{exc} = 410 nm) of PYTG (0.5 μM) with varying solvent polarity.

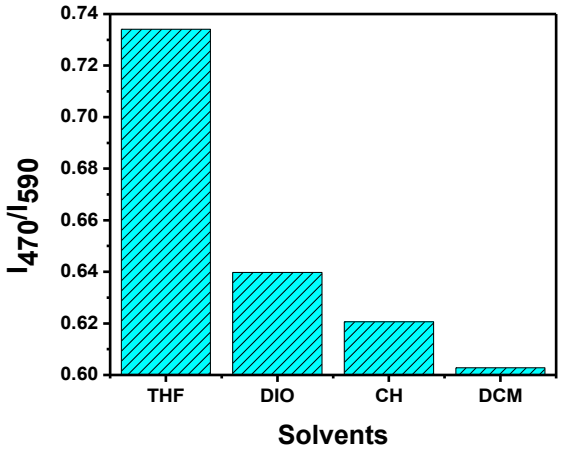

Fig. S4 Emission intensity of the monomer to that of the excimer with varying the solvent polarity.

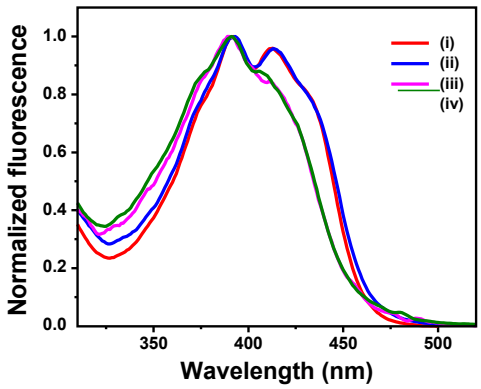

Fig. S5 Fluorescence excitation spectra of PYTG in (i) DCM (λ_{em} = 590 nm), (ii) $CHCl_3$ (λ_{em} = 590 nm), (iii) dioxane (λ_{em} = 582 nm) and (iv) THF (λ_{em} = 568 nm).

(b) Fluorescence quantum yield measurements:

The fluorescence quantum yield of PYTG was estimated using coumarin 102 as a standard dye in ethanol (Φ_f = 76%) and was calculated using the equation 1.[S6] The quantumyields of PYTG in different solvents were listed in Table S1.

$$\Phi_{F_{X}} = \Phi_{f,x} \frac{*}{F_S} * \frac{f_S}{f_x} * \frac{n_X^2}{n_S^2} \quad \ldots\ldots (1)$$

where, Φ_f is the fluorescence quantum yield, the subscript x denotes sample, and the subscript s refers to the standard, F denotes integral fluorescence, n refers to the refractive index of the solvent used in the measurements and f is the absorption factor at the excitation wavelength given by the following equation: $f = 1 - 10^{-A(\lambda_{ex})} = 1 - 10^{-\varepsilon(\lambda_{ex})}$, where A is the absorbance and ε molar extinction coefficient in L mol^{-1} cm^{-1}.

Table S1 Spectroscopic data of PYTG (0.5 μM) in various organic solvents are shown.

Solvent	Absorption	Fluorescence	
	λ_{max} (nm)	λ_{em} (nm)	Quantum yield (%)
Chloroform	392, 410	470, 590	26
DCM	392, 414	465, 590	20
THF	402	465, 568	1
Dioxane	410	465, 582	3
Acetonitrile	411	Very less intensity	NM
N,N-Dimethylformamide	410	Very less intensity	NM
Dimethyl sulfoxide	413	Very less intensity	NM

*NM: not measured

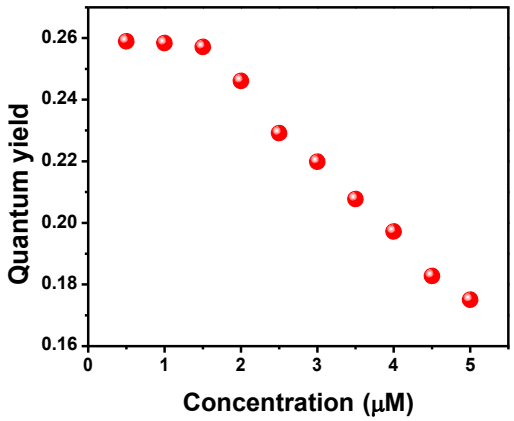

Fig. S6 Variation of fluorescence quantum yields of PYTG with increasing concentration in chloroform (0.5 – 5 μM).

The quantum yields of PYTG (in $CHCl_3$) decreased with increasing concentration in the range of 0.5 μM to 5 μM (Fig. S6). Fig. S3b reveals the formation of excimer of PYTG in chloroform even at 0.5 μM concentration. Thus, the unusual variation of fluorescence quantum yields of PYTG with increasing concentration may depend on the nature of the excimer. Hence, we probed the formation of excimer of PYTG through excitation spectra, lifetime and time-resolved emission spectra measurements to elucidate the underlying photophysics behind the above observation.

(c) Fluorescence lifetime measurements:

The excited state behavior of PYTG was monitored using TCSPC technique. Lifetime measurement of PYTG was carried out exciting with a 408 nm diode laser and monitoring the emission at monomer (λ_{em} = 470 nm) and excimer (λ_{em} = 590 nm) emission peaks in two different solvents (DCM and $CHCl_3$). The triexponential decay profile of PYTG (Fig. S7) suggests the presence of multiple emissive species possibly arising due to monomer, π-conjugated delocalized state and excimer (intra and/ or intermolecular). Table S2 reflects that the slower decay time of PYTG at excimer emission in both the solvents as compared to that of the monomer emission.

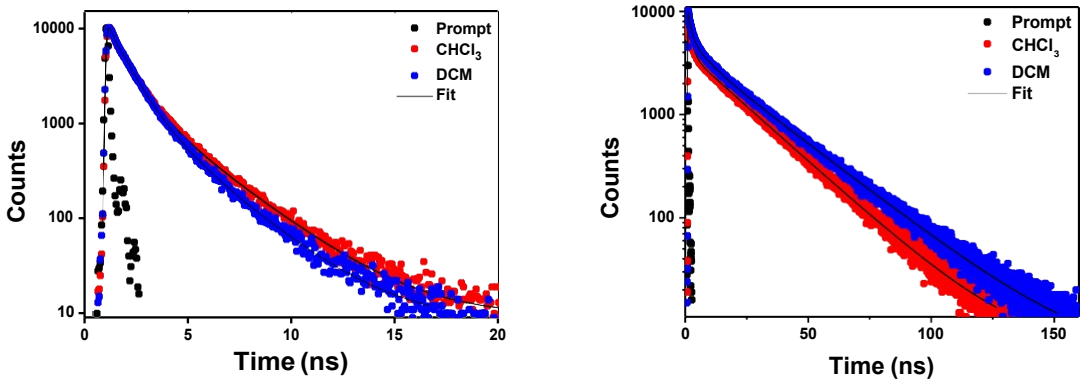

Fig. S7 Fluorescence decay profiles (λ_{exc} = 408 nm) of PYTG in (a) $CHCl_3$ (monomer emission: λ_{em} = 470 nm) and DCM (monomer emission: λ_{em} = 465 nm), (b) $CHCl_3$ (excimer emission: λ_{em} = 590 nm) and DCM (excimer emission: λ_{em} = 590 nm).

Table S2 Fluorescence decay parameters of PYTG (λ_{exc} = 408 nm) in $CHCl_3$ and DCM; the decay times (τ_1, τ_2, and τ_3) and the respective fractional contributions (α_1, α_2 and α_3), the weighted average decay time ($\tau_{avg.}$) and the quality of fitting (χ^2) are shown.

Entry	λ_{em} (nm)	Decay parameters							
		τ_1 (ns)	α_1	τ_2 (ns)	α_2	τ_3 (ns)	α_3	$\tau_{avg.}$ (ns)	χ^2
$CHCl_3$	470	0.2	7	0.9	49	2.7	44	2.0	1.04
	590	1.3	6	6.6	9	23.8	85	19	1.08
DCM	465	0.2	6	0.9	58	2.5	36	1.7	1.00
	590	0.2	1	1.6	8	20.3	91	18.6	1.15

(d) Concentration dependent excimer formation:

Basic spectroscopic investigations revealed the dual emissive nature of PYTG with two distinct and well-separated emission bands (monomer and excimer). Hence, we thought to investigate the spectral features of PYTG through the perturbation of its environment via varying the concentration, temperature, pH of the medium and addition of the external ions.[17-24] In this context, at first, the monomer and excimer emission bands were monitored with varying the concentration of the PYTG from 0.5 μM to 5 μM in $CHCl_3$. A noticeable increment of the excimer emission was observed as compared to that of the monomer emission with increasing the concentration of the PYTG (Fig. S8). Fig. S9 reflects the facile formation of the excimer over to that of the monomer with increasing concentration of the PYTG. Fig. S10 depicts the CIE chromaticity diagram of PYTG in comparison with pyrene with varying concentration from 0.5 μM to 5 μM.

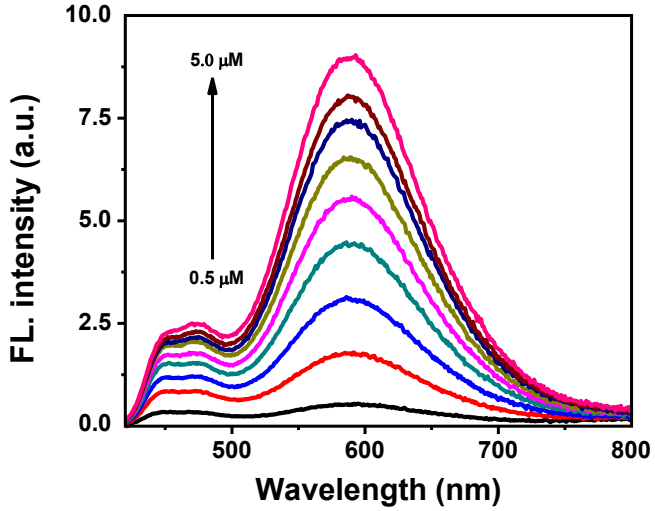

Fig. S8 Emission spectra (λ_{exc} = 410 nm) of PYTG recorded in $CHCl_3$ with varying the concentration from 0.5 μM to 5 μM.

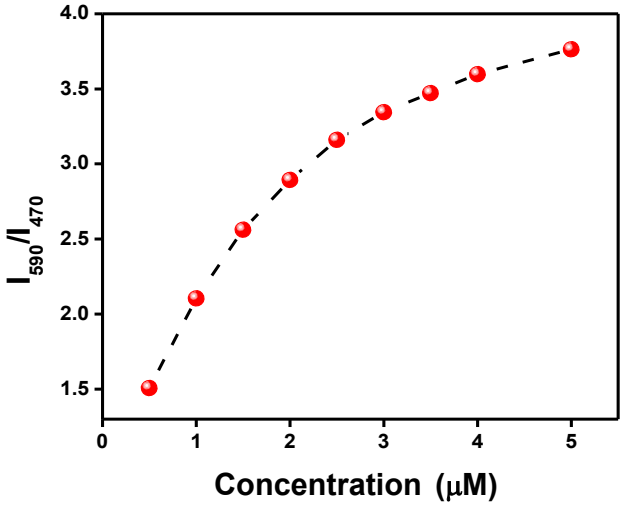

Fig. S9 The plot of fluorescence intensity ratio (λ_{exc} = 410 nm) of excimer to that of the monomer (I_{590}/I_{470}) with respect to the concentration of PYTG in $CHCl_3$.

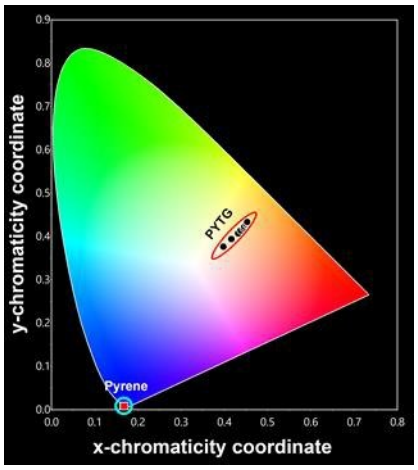

Fig. S10 The CIE chromaticity diagram of PYTG and pyrene with varying concentration (0.5 µM to 5 µM).

The nature of the excimer (dynamic or static) was probed through monitoring the excitation spectra at monomer emission (470 nm) and excimer emission (590 nm). The results revealed that the features of the excitation spectra for both cases were almost similar indicating the formation of dynamic excimer (Fig. S11).

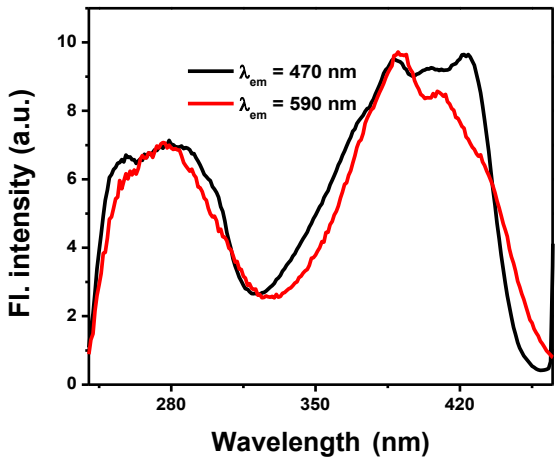

Fig. S11 Excitation spectra of PYTG (5 µM in $CHCl_3$) recorded at 470 nm (monomer emission) and 590 nm (excimer emission).

Table S3 Fluorescence decay (λ_{exc} = 408 nm) parameters with varying concentration (0.5 μM to 5 μM) of PYTG in $CHCl_3$; the decay times (τ_1, τ_2, and τ_3, ns) and the respective fractional contributions (α_1, α_2 and α_3), the weighted average decay time (τ_{av}, ns) and the quality of fitting (χ^2) are shown. The respective emission wavelengths (nm) are indicated.

Concentration (μM)	**Decay parameters**									
(λ_{exc} = 408 nm)	$\tau_1(\alpha_1)$		$\tau_2(\alpha_2)$		$\tau_3(\alpha_3)$		$\tau_{avg.}$		χ^2	
	470	590	470	590	470	590	470	590	470	590
0.5	0.3 (3.3)	1.3 (38.4)	0.7 (84.4)	6.2 (13.8)	2.5 (12.3)	24.0 (47.6)	0.9	12.8	1.17	1.20
1.0	0.3 (5.4)	1.4 (35.9)	0.7 (76.1)	8.6 (13.5)	2.5 (18.4)	25.3 (50.5)	1.0	14.4	1.18	1.06
1.5	0.2 (5.1)	1.34 (16.0)	0.8 (73.6)	6.0 (9.4)	2.5 (21.2)	24.5 (74.4)	1.1	19.0	1.18	1.13
2.0	0.2 (3.1)	1.3 (12.7)	0.8 (70.0)	6.7 (9.4)	2.4 (26.8)	25.3 (77.7)	1.2	20.5	1.02	1.15
2.5	0.3 (8.8)	1.3 (10.8)	0.8 (67.1)	7.9 (8.2)	2.5 (24.0)	25.6 (80.8)	1.2	21.5	1.15	1.15
3.0	0.3 (6.9)	1.2 (8.2)	0.8 (66.9)	8.3 (8.2)	2.5 (26.0)	25.6 (83.3)	1.2	22.1	1.13	1.16
4.0	0.3 (6.2)	1.4 (6.3)	0.8 (66.8)	12.8 (12.9)	2.5 (26.9)	26.5 (80.6)	1.2	22.5	1.06	1.18
5.0	0.3 (6.2)	1.4 (6.3)	0.8 (66.8)	12.8 (12.9)	2.5 (26.9)	26.5 (80.6)	1.2	23.1	1.06	1.18

Lifetime measurements of PYTG were carried out exciting with a 408 nm diode laser and monitoring at monomer (λ_{em} = 470 nm) and excimer (λ_{em} = 590 nm) emission peaks with varying the concentration from 0.5 μM to 5 μM (Fig. 3, main text). The amplitude average decay time was similar at monomer emission while significantly increased at the excimer emission with increasing concentration (Table S3). This result eventually proved the formation of the dynamic excimer with the increasing concentration of PYTG.

The dynamic nature of the excimer was also probed through the time-resolved emission spectra (TRES) measurements. TRES measurement of PYTG (5 μM, $CHCl_3$) was carried out at room temperature and the emission profiles were collected at different delay time (up to 25.2 ns) in the wavelength range from 425 to 700 nm at 5 nm interval. At lower delay time, an intense peak was observed in the region of 460 to 470 nm. Whereas, with the increases of the delay time, a predominant peak was noticed in the region of 560 to 570 nm. These observations revealed the formation of dynamic excimer with increasing the concentration of PYTG (Fig. 4a, main text, Fig. S12).

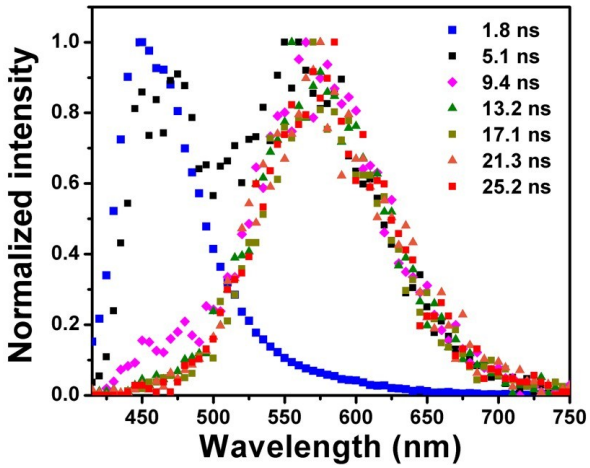

Fig. S12 Time-resolved emission spectra (TRES) of PYTG in $CHCl_3$ (5 μM) using picosecond pulsed diode laser (EPL- 408 nm) as an excitation source depicting the dynamic nature of the PYTG excimer.

The excitation (Fig. S11), decay time (Table S3) and time-resolved emission spectra (Fig. S12) measurements clearly suggested the formation of dynamic excimer with the increasing concentration of PYTG. Thus, the decrease of fluorescence quantum yield with increasing concentration can be inferred to the nonradiative deactivation due to the formation of dynamic excimer (Fig. S6). This result indicates that the excimer formation of PYTG mostly governed by the intramolecular interactions at lower concentration regime.

VI. Effect of temperature

The temperature-dependent fluorescence measurements were carried out in quartz cuvettes of 1 cm path length, fitted in a cuvette holder thermally equilibrated using a Newport Peltier thermostat (Newport Corporation, USA, Model No. 350B). Measurements were performed in the temperature range of -10 to 55 °C. The temperature was further verified using IR thermometer before and after taking the emission spectra. The variation of temperature for each measurement was within ± 2 °C.

The temperature effect on the excimer formation of PYTG ($CHCl_3$) was carried out with both 5 µM and 0.5 µM solutions. Fig. 4b (main text) and Fig. S13-S15 display the emission profile of PYTG largely dependent upon the temperature. At lower temperature (263 K), PYTG exhibited emission bands at 602 nm and 470 nm, which were assigned to the excimer and monomer emission, respectively. The excimer formation of PYTG (5 µM) was further proved through the Stevens-Ban plot (Fig. S13) which revealed an intersection point between the lower and higher temperature regimes indicating the dynamic nature of the excimer.[25] A significant decrease in the excimer emission around 602 nm was also observed at a lower concentration (0.5 µM) with the increase of temperature from 263 K to 328 K. Whereas, a very less significant change was observed at monomer emission band (470 nm, Fig. S14). The emission intensity of excimer to monomer (I_{602}/I_{470}) against temperature was shown in Fig. S15. Hence, the effect of temperature on excimer emission of PYTG may be elucidated by considering the formation of excimer at a lower temperature which is dynamic in nature.

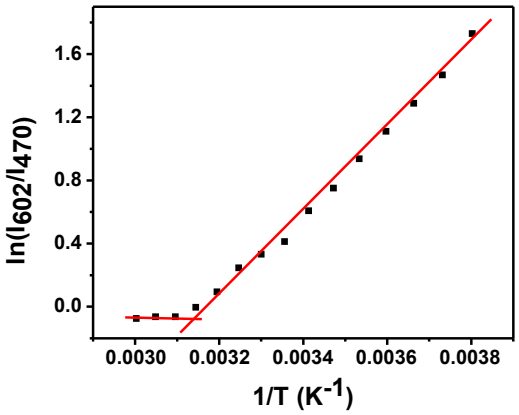

Fig. S13 Stevens-Ban plot of $\ln(I_{602}/I_{470})$ against reciprocal of the absolute temperature of PYTG (5 µM, $CHCl_3$, λ_{exc} = 410 nm).

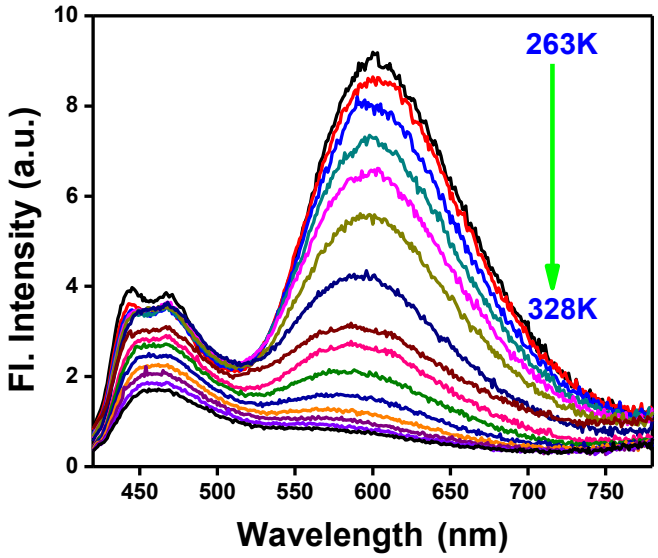

Fig. S14 Fluorescence emission (λ_{exc} = 410 nm) spectra of PYTG (0.5 μM in $CHCl_3$) with varying the temperature from 263 K to 328 K.

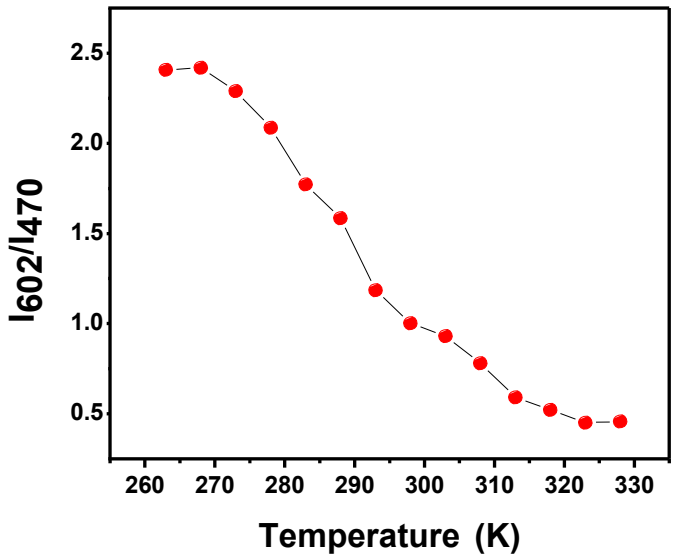

Fig. S15 I_{602}/I_{470} (fluorescence emission intensity ratio of excimer to that of the monomer) against the absolute temperature plot of PYTG (0.5 μM in $CHCl_3$) at λ_{exc} = 410 nm.

VII. Excimer assisted white light emission

The quality of white light can be judged by three individual parameters discussed below.

(a) The quality of white light was characterized by the Commission Internationale de I'Eclairage (CIE) chromaticity coordinates (x, y) revealing the emission color in the chromaticity diagram. A pure and perfect white light system has CIE coordinates (x = 0.33, y = 0.33), whereas a quite broad region around this point in the diagram can be considered as white light.[26,27]

(b) The color rendering index (CRI) is a numerical value ranging from 0 - 100, which measures the true color of the object when illuminated by a light source. CRI value for WLE systems are preferably higher than 80.[28] The quality of the color, which can be distinguishable from one to another, is given by Munsell color system. The different hue of the colors is designated by code (R_n.). The general CRI is indicated by symbol R_a which is the average value of R_1 to R_n.

(c) The broad band light source is characterized by the correlated color temperature (CCT) and it is defined as the temperature of the black body radiator, which emits the same color as that of the light source. For lighting application, CCT range is usually 2500-6500 K.[25,27] The CCT values are calculated using McCamy's formula.[29]

The CIE coordinates, CRI and CCT were calculated using ColorCalculator 6.31 from Osram Sylvania, Inc. using the corrected emission spectra.

PYTG exhibits yellowish-orange fluorescence with the peak centred at 590 nm and a shoulder band at 470 nm (main text, Fig. 1a). The emission colour was tuned by varying the concentration from 0.1 μM to 3 μM. The pure white light emission was obtained at 1.5 μM of PYTG in DCM. A broad emission ranging from 425 to 750 nm was obtained when excited at 410 nm (main text, Fig. 5a). At 1.5 μM of PYTG, the equal contributions of monomer and excimer emissions, leading to the pure white light emission with CIE coordinates (0.33, 0.34). The CRI (R_a) value of WLE solution was found to be 85 (Fig. S16) and CCT was 5438 K.

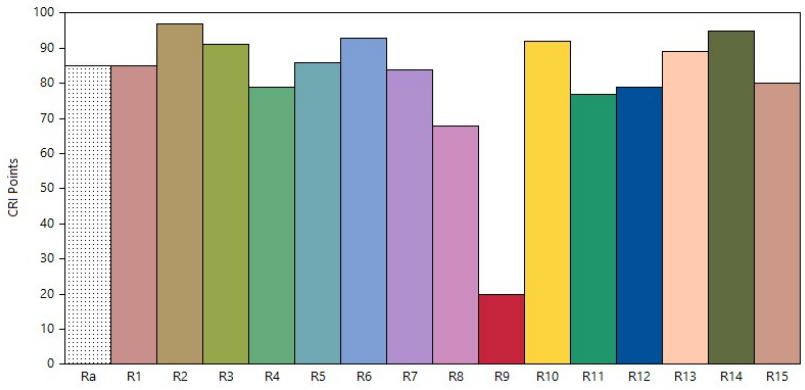

Fig. S16 The CRI of WLE solution of PYTG (1.5 μM in DCM) at various Munsell codes.

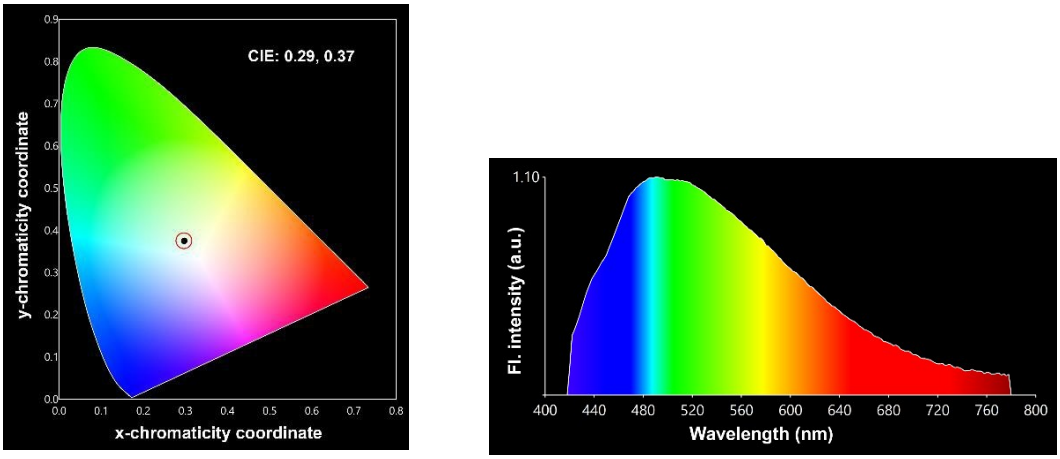

Fig. S17 The CIE chromaticity diagram of PYTG (1.5 μM) in PMMA polymer matrix (1g/ 3 mL DCM) and corresponding emission spectrum (λ_{exc} = 410 nm) of PYTG.

The emission behavior of PYTG in PMMA/DCM solution was also checked (Fig. S17). The white light emission of PYTG in PMMA/DCM solution was likely to be due to the high viscous nature of the medium preventing the nonradiative relaxations. However, the CIE coordinates of PYTG (1.5 μM) in pure DCM, PMMA/DCM (1 g PMMA in 3 mL DCM) solution and in thin film (same concentration of PYTG and PMMA) were found to be slightly different and respectively, (0.33, 0.34), (0.29, 0.37) and (0.33, 0.38). The variation of CIE coordinates in PMMA matrix can be contributed by specific interactions with heteroatoms and the effect of rigid environments.

VIII. Colorimetric detection of fluoride ion

We assumed that the electron deficient central carbon moiety might react with an external anion to stabilize the whole system and alter the photophysical behaviour of PYTG. 1 mM stock solution of PYTG was prepared in DMSO and subsequently diluted for further studies. The addition of tetrabutylammonium fluoride (TBAF) salt to PYTG solution exhibited a drastic colour change from light yellow to dark blue as compared to that of the other anions viz., AcO^-, BzO^-, I^-, Cl^-, Br^-, HPO_4^{2-}, $H_2PO_4^-$, and HSO_4^- (Fig. S18a). The addition of TBAF salt (1 mM) to PYTG solution (3 μM) exhibited a new absorption band around 596 nm while no change in the absorption spectra was observed with other analytes (Fig. S18b). The UV–Vis. titration experiment was carried out with F^- (Fig. S18c). Two clear isosbestic points at 350 and 470 nm were observed. The dark blue colour is due to the formation of the new chemical species through the deprotonation of –NH group by fluoride ions. The lowest detection limit was calculated from the UV-Vis. titration data and was found to be 2.9 μM with the linearity range of 18 to 33 mM (Fig. S19).

To identify the possible anion binding mode, ^{1}H NMR titration [in DMSO-d_6 (3.5 μM)] was performed (Fig. S20). The signal at 12.52 ppm which is assignable to the N-H proton of PYTG disappeared after addition of TBAF salt and other remaining aromatic protons were broadened and upfield shifted. The aldimine proton –CH=N– (10.08 ppm, H_b) along with aromatic proton Ar-H_c (9.19 ppm, H_c) shows a slightly upfield shift ($\Delta\delta$ = 0.14 and 0.07 ppm for aldimine and Ar-Hc, respectively) while the other aromatic proton (Ar-H_d, 8.60 ppm) showed downfield shift ($\Delta\delta$ = 0.14 ppm) which suggests the interaction of fluoride with PYTG through hydrogen bonding. On further addition of 5 equiv. of fluoride, the Ar-H_d signal shifted further to downfield ($\Delta\delta$ = 0.33 ppm) while the signal for Ar-H_c and aldimine proton –CH=N– upfield shifted ($\Delta\delta$ = 0.20, 0.51 ppm, respectively). The deprotonation of –N-H of PYTG led to an increase in electron density over the phenyl ring, so the resonances for the –CH=N– as well as aromatic protons except Ar-H_d displayed noticeable upfield shifts (Fig. S20). Thus, ^{1}H NMR studies support the sensing of F^- by PYTG through hydrogen bonding between -NH and F^- leading to the deprotonation. Additionally, we carried out the UV-visible absorption titration of PYTG in the presence of a base (tetrabutylammonium hydroxide) to ensure the mechanism of colorimetric sensing of the fluoride ion (Fig. S21). The change in absorption spectra was found to be similar as observed upon addition of fluoride ions (Fig. S18c). This data further supports that the colorimetric sensing of fluoride ion is due to the deprotonation of PYTG.

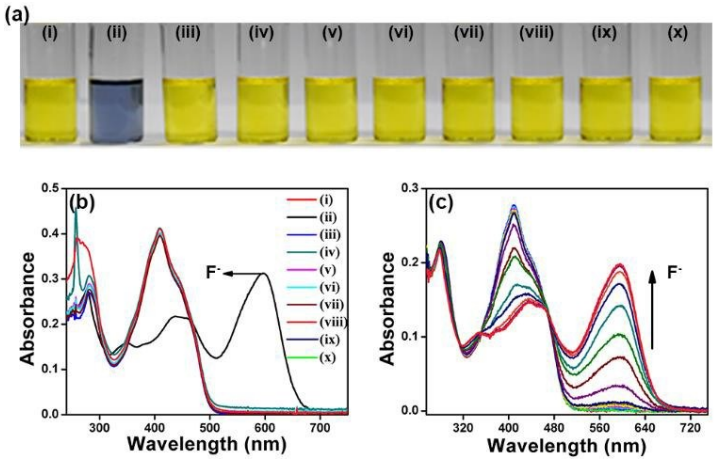

Fig. S18 (a) The visible color change of PYTG (i) native solution (3 μM, DMSO) and in the presence of different anions (1 mM): (ii) F^-, (iii) Cl^-, (iv) Br^-, (v) I^-, (vi) AcO^-, (vii) BzO^-, (viii) $H_2PO_4^-$, (ix) HPO_4^{2-} and (x) HSO_4^-. (b) Absorption spectra of PYTG (3 μM, DMSO) with the addition of different anions (1 mM, DMSO) and (c) absorption titration profile of PYTG (3 μM, DMSO) with varying concentration of F^-.

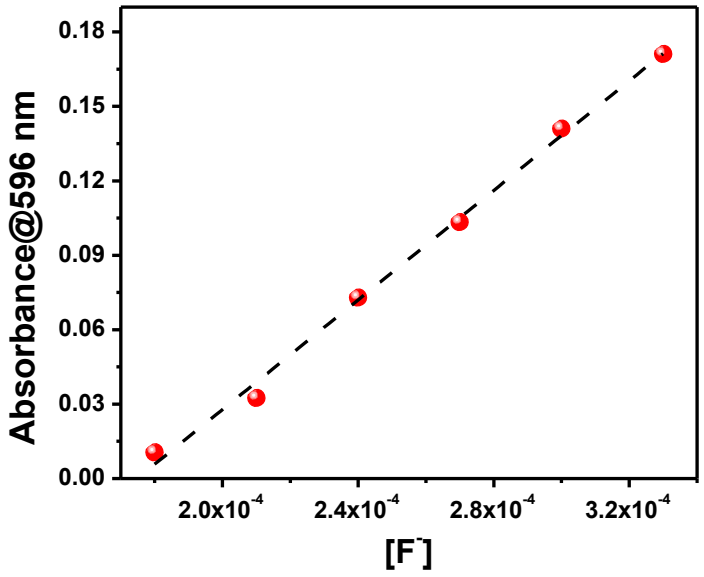

Fig. S19 Absorbance at 596 nm vs. fluoride ion concentration plot.

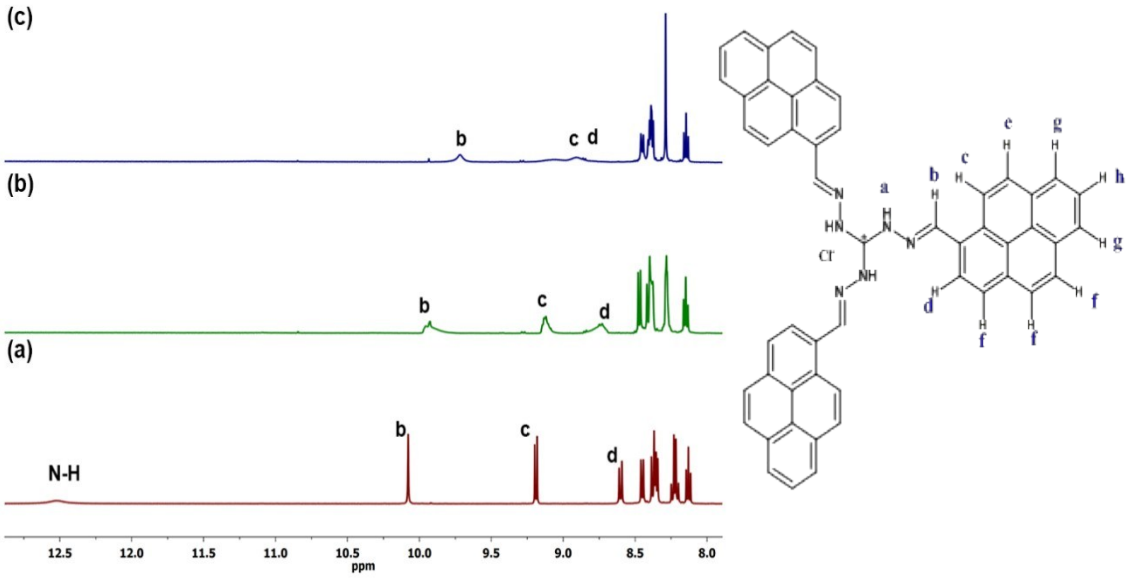

Fig. S20 ^{1}H NMR titration of PYTG with F^- in DMSO-d_6 at room temperature: (a) PYTG, (b) PYTG + 3 eqv. of F^-, (c) PYTG + 5 eqv. of F^-.

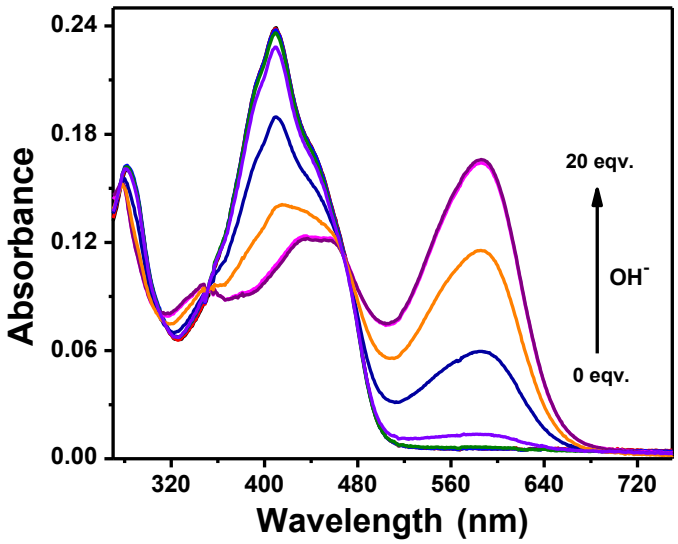

Fig. S21 Absorption titration of PYTG (3 μM in DMSO) with varying concentration of tetrabutylammonium hydroxide (0 to 20 eqv.).

IX. Aggregation behavior of PYTG

The aggregation behaviour of PYTG was checked in acetonitrile (MeCN) with varying the water fraction. Absorption spectra of PYTG (5 μM) were recorded in different MeCN-water mixtures. The absorption of PYTG showed a band around 412 nm in dilute MeCN solution and remains unchanged with increasing the water fraction up to 40% (Fig. S22). The peak was then found to be blue shifted (393 nm) with increasing the water fraction from 50% to 90%.

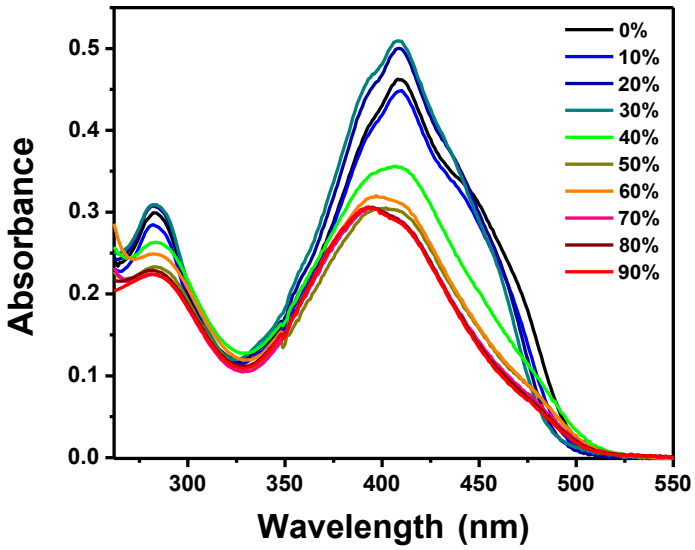

Fig. S22 UV-Visible absorption spectra of PYTG (5 μM) in MeCN-water with varying the fraction of water from 0% to 90%.

Similarly, the fluorescence spectra of PYTG (5 μM, MeCN) with varying the water fraction was monitored and a blue-shifted emission band at 460 nm was noticed (Fig. S23a) with increasing the water fraction (more than 40%). Fig. S23b reflects the variation of fluorescence intensity with the increasing fraction of water. The dramatic increase of fluorescence intensity was found to be due to the formation of pyrene aldehyde generated through hydrolysis of Schiff base.[30] The similar fluorescence response was observed with pyrene aldehyde (5 μM) in MeCN-water mixture with increasing percentage of water (Fig. S24). The blue fluorescence was due to the formation of spherical nanoaggregates of pyrene aldehyde as revealed by the FESEM images (Fig. S25).

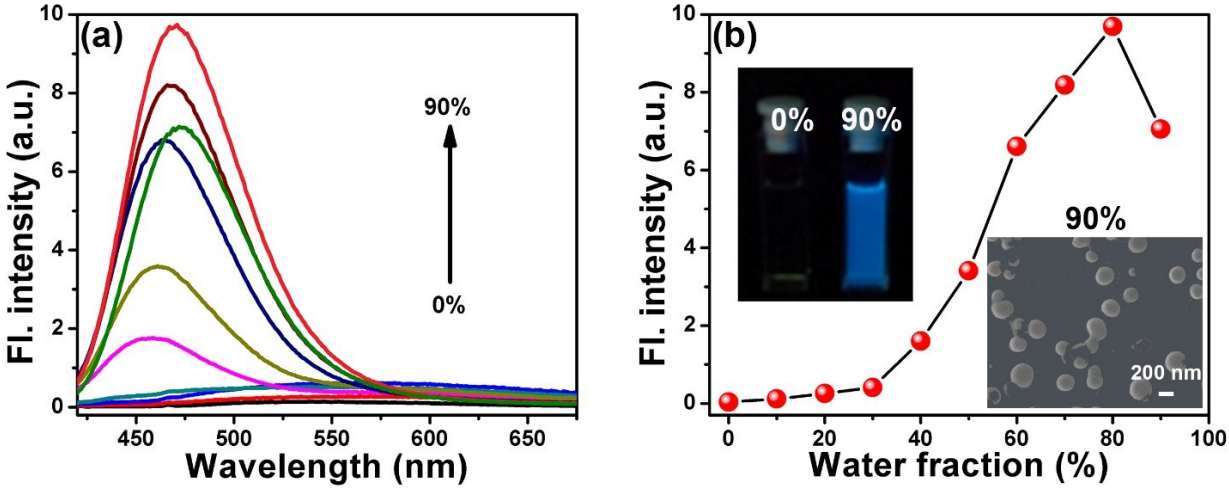

Fig. S23 (a) Fluorescence spectra (λ_{exc} = 410 nm) of PYTG (5 μM) in MeCN-water with increasing water fraction (0 – 90%). (b) The plot of fluorescence intensity (at 470 nm) vs fraction of water; inset: digital photographs of PYTG solution with 0% and 90% water fraction under the illumination of UV light (λ_{exc} = 365) nm and FESEM image of the PYTG dispersion in MeCN:H_2O = 1:9.

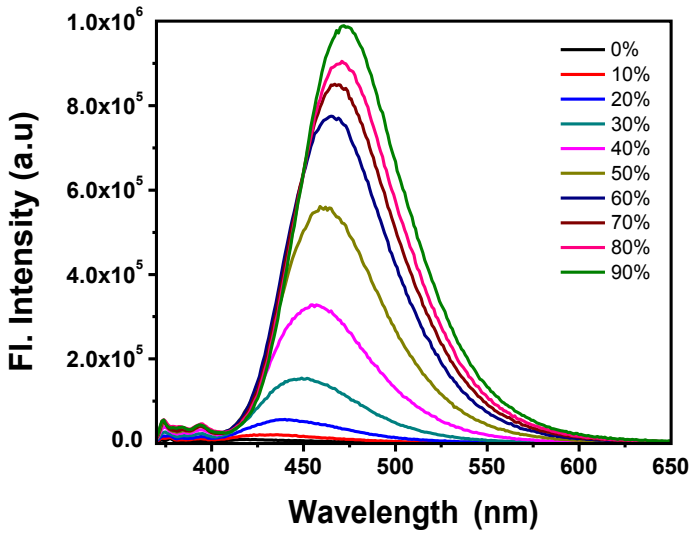

Fig. S24 Fluorescence spectra (λ_{exc} = 410 nm) of pyrene aldehyde (5 μM, MeCN-H_2O) with increasing the fraction of water.

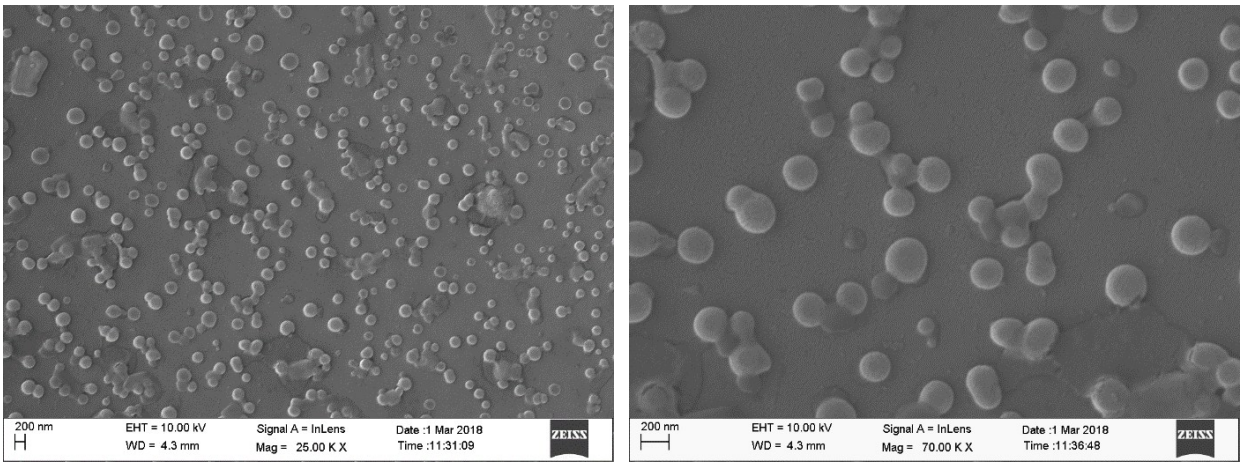

Fig. S25 FESEM images of PYTG dispersion (5 μM, 80% water and 20% MeCN).

X. Effect of acid and base

Photophysical properties of PYTG were also monitored in the presence of acidic (trifluoroacetic acid, TFA) and basic (triethylamine, TEA) environments. 10 µL TFA was added to PYTG solution (3 mL, 5 µM, $CHCl_3$) resulting in the pH of the medium ~ 2. The excimer emission was found to be slightly red-shifted (Fig. S26). Whereas, a complete new feature and a significant decrease of fluorescence intensity were noticed upon addition of TEA (10 µL) to the solution of PYTG (3 mL, 5 µM, $CHCl_3$, pH ~ 10). At a higher pH, new chemical species are likely to be formed due to deprotonation.

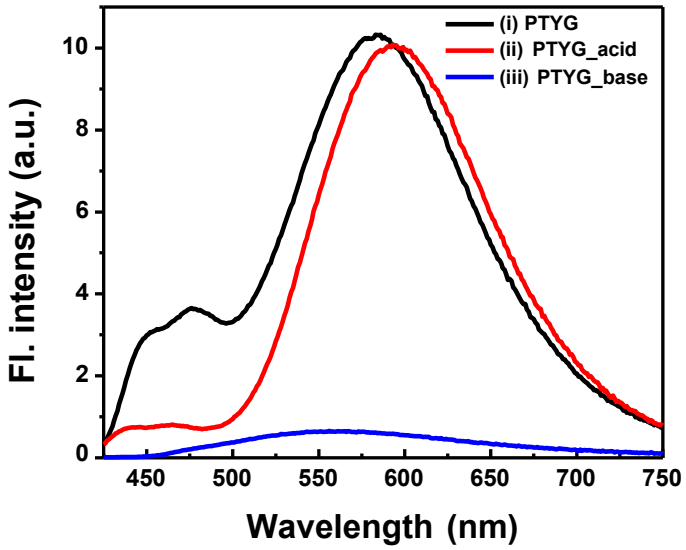

Fig. S26 Fluorescence spectra of (i) PYTG (in $CHCl_3$, λ_{exc} = 410 nm), (ii) PYTG in the presence of 10 µL of trifluoroacetic acid (pH ~ 2, in $CHCl_3$, λ_{exc} = 415 nm) and (iii) PYTG in the presence of 10 µL of triethylamine (pH ~ 10, in $CHCl_3$, λ_{exc} = 400 nm).

XI. Static excimer formation and detection of trivalent metal ions

The presence of three coordinating sites and electron-rich property of PYTG motivated us to monitor its excimer behavior in the presence of external metal ions. It was expected that in the presence of some cationic species, the electron rich nitrogen centers of PYTG might coordinate with suitable electron deficient analytes. Hence, a 1.0×10^{-3} M stock solution of PYTG was prepared in acetonitrile (MeCN) and diluted with semi-aqueous mixture of MeCN: H_2O in a ratio of 3:2 v/v to 3.0×10^{-6} M. Aqueous solutions of Na^+, K^+, Mg^{2+}, Mn^{2+}, Fe^{2+}, Co^{2+}, Ni^{2+}, Cu^{2+}, Zn^{2+}, Cd^{2+}, Hg^{2+}, Pb^{2+}, Fe^{3+} Al^{3+} Cr^{3+} ions were prepared from respective chloride salts.

A noticeable change in UV-Visible absorption spectra of PYTG (3 μM, MeCN:H_2O; 3:2) observed only in the presence of Fe^{3+} and Al^{3+} exhibiting three characteristic bands at 409 nm, 390 nm and 282 nm (Fig. S27). The emission behavior of PYTG in the presence of respective metal ions was checked. PYTG was found to be selective only towards Fe^{3+}/Al^{3+} with a turn on fluorescence signal (Fig. 6a, main text). The enhancement of the excimer emission peak at 590 nm might be due to the strong chelation-enhanced fluorescence (CHEF) upon addition of trivalent Fe^{3+}/Al^{3+} to PYTG. The chelation of PYTG induces the molecular rigidity and inhibits the cis-trans isomerization across the aldimine bond reducing the nonradiative deactivation. The fluorescence titration experiments using 3 mL aliquot of PYTG solution (3 μM, MeCN:H_2O; 3:2) were performed in the presence of Fe^{3+}/Al^{3+} (up to 5 eqv.). Each spectrum was acquired after 1 min of the addition of metal ions. A drastic enhancement of the emission intensity of PYTG was observed with increasing concentration of Fe^{3+} and Al^{3+} (Fig. 6b, main text and Fig. S28).

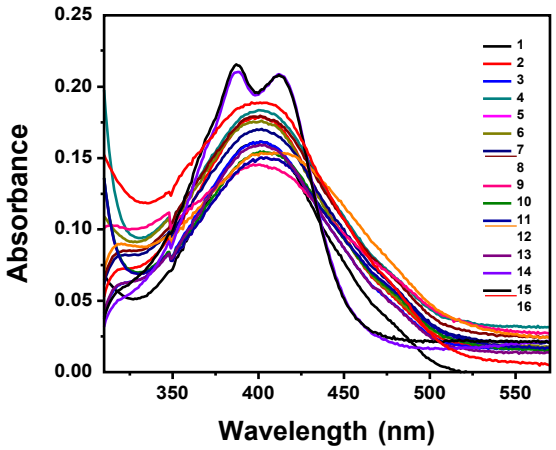

Fig. S27 Absorption spectra of 3 μM PYTG in the presence of different metal ions (5 eqv.) in semi-aqueous solution (MeCN : H_2O; 3:2, v/v). Figure legends: 1: PYTG, 2: Na^+, 3: K^+, 4: Mg^{2+}, 5: Mn^{2+}, 6: Fe^{2+}, 7: Co^{2+}, 8: Ni^{2+}, 9: Cu^{2+}, 10: Zn^{2+}, 11: Cd^{2+}, 12: Hg^{2+}, 13: Pb^{2+}, 14: Fe^{3+}, 15: Al^{3+}, 16: Cr^{3+}.

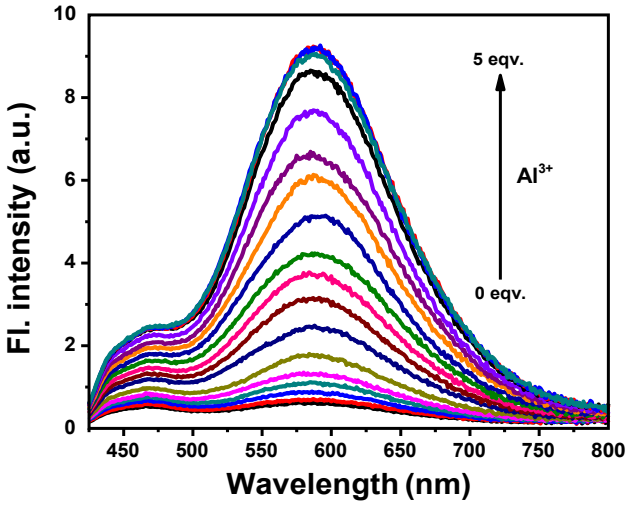

Fig. S28 Emission spectra (λ_{exc} = 410 nm) of 3 μM PYTG in semi-aqueous solution (MeCN:H_2O; 3:2, v/v) with varying concentration of Al^{3+} ions (0 to 5 eqv.).

Estimation of the detection limit:

In general, the Limit of Detection (LOD) is taken as the lowest concentration of an analyte in a sample that can be detected. The detection limit is calculated using the equation 2.[31] Table S4 shows the limit of detection (LOD) of PYTG towards the metal ions. Fig. S29 and S30 reveal the chelation-enhanced fluorescence nature of PYTG in the presence of Fe^{3+} and Al^{3+}, respectively. The binding stoichiometries of Fe^{3+} and Al^{3+} with PYTG were determined through JOB's plot by the method of continuous variation (Fig. S31 and S32).[32]

$$\text{Limit of Detection (LOD)} = 3\sigma/m \quad \ldots\ldots\ldots\ldots\ldots\ldots \quad (2)$$

where, σ is the standard deviation of the solution of receptor without any analyte and m is the slope between absorbance or fluorescence intensity vs. the concentration of the analyte.

Table S4 The lowest detection limit of PYTG towards the metal ions.

Entry	Limit of detection (M)	R^2	Linearity range (M)
PYTG-Fe^{3+}	5.4×10^{-9}	0.994	2.6×10^{-6} - 1.2×10^{-5}
PYTG-Al^{3+}	14×10^{-9}	0.999	1.0×10^{-5} - 3.0×10^{-5}

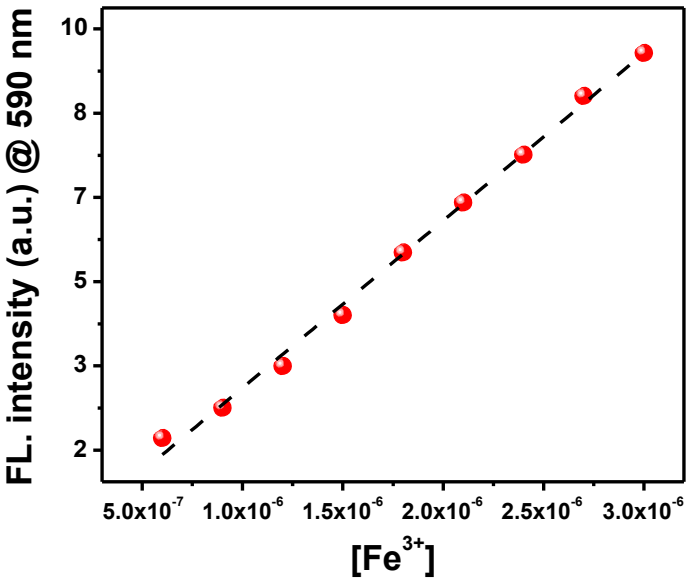

Fig. S29 The plot of fluorescence intensity (λ_{em} = 590 nm) of PYTG (3 μM, MeCN:H_2O; 3:2, v/v) vs. concentration of Fe^{3+}.

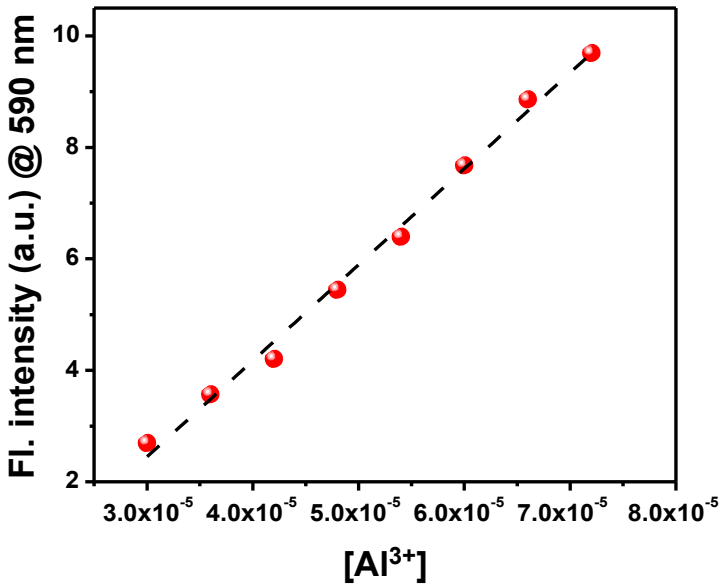

Fig. S30 The plot of fluorescence intensity (λ_{em} = 590 nm) of PYTG (3 μM, MeCN:H_2O; 3:2, v/v) vs. concentration of Al^{3+}.

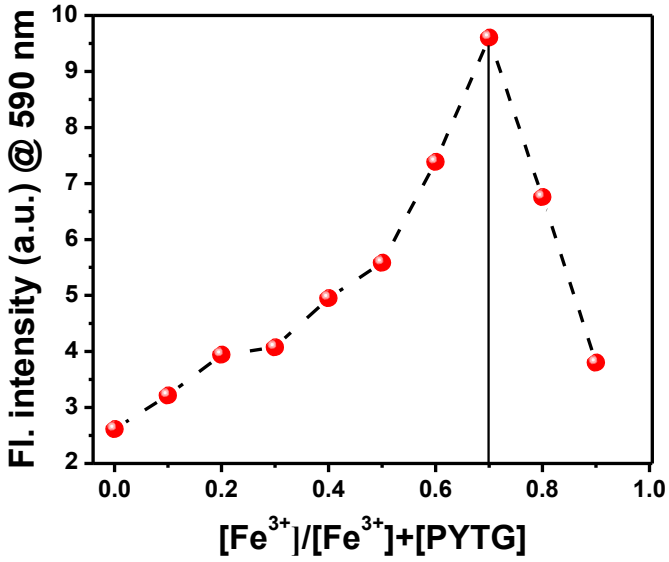

Fig. S31 Job's plot showing the 1:3 stoichiometry of the complex between PYTG (3 µM, in MeCN:H_2O; 3:2, v/v) and Fe^{3+}. The total concentration of PYTG and Fe^{3+} mixture was kept at 10 µM.

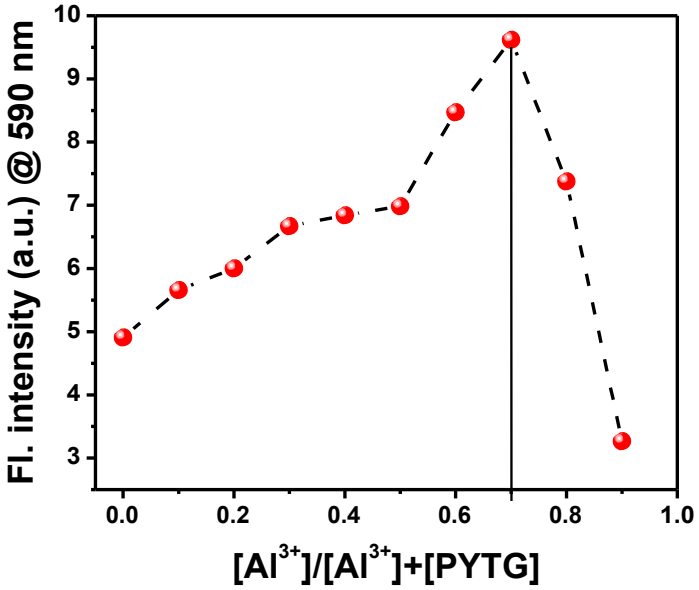

Fig. S32 Job's plot showing the 1:3 stoichiometry of the complex between PYTG (3 µM, in MeCN:H_2O; 3:2, v/v) and Al^{3+}. The total concentration of PYTG and Al^{3+} mixture was kept at 10 µM.

Determination of association constant:

The association constants were determined by a nonlinear least-square analysis of fluorescence intensity (I) versus concentration of the metal ion (C_M or [M]) using the equation 3, reported for multiple ligand systems.[33,34]

$$I = \frac{I_0 + c_M\varphi_1 K_{11}[M] + c_M\varphi_2\beta_{21}[M]^2 + I_{\square i \square}\beta_{31}[M]^3}{1 + K_{11}[M] + \beta_{21}[M]^2 + \beta_{31}[M]^3} \quad \ldots\ldots\ldots\ldots\ldots\ldots (3)$$

Where $\beta_{21} = K_{11}K_{21}$, $\beta_{31} = K_{11}K_{21}K_{31}$, $[M] \approx C_M$ is Fe^{3+}/Al^{3+} concentration, I_0 and I is integrated emission in the absence and presence of Fe^{3+}/Al^{3+} ion, respectively. Φ_1 is approximately 0.042, the quantum yield of the 1:1 PYTG-Fe^{3+} complex; Φ_2 is approximately 0.069, the quantum yield of the 1:2 PYTG-Fe^{3+} complex. By plotting the fluorescence intensity at 590 nm of PYTG (ligand, L) versus increasing concentration of [Fe^{3+}/ Al^{3+}], sigmoidal curves were obtained and the corresponding association constants were deduced (Fig. S33 and S34). The association constants of PYTG (single ligand system) with Fe^{3+} and Al^{3+} were found to be $K_{11} = 1.2\times10^5$, $K_{12} = 4.2\times10^5$, $K_{13} = 4.8\times10^5$ for Fe^{3+} and $K_{11} = 1.1\text{x}10^5$, $K_{12} = 2.9\text{x}10^5$, $K_{13} = 8.8\text{x}10^5$ for Al^{3+} respectively. Fig. S35 reveals the reversible chelation behaviour of PYTG towards Al^{3+} ions.

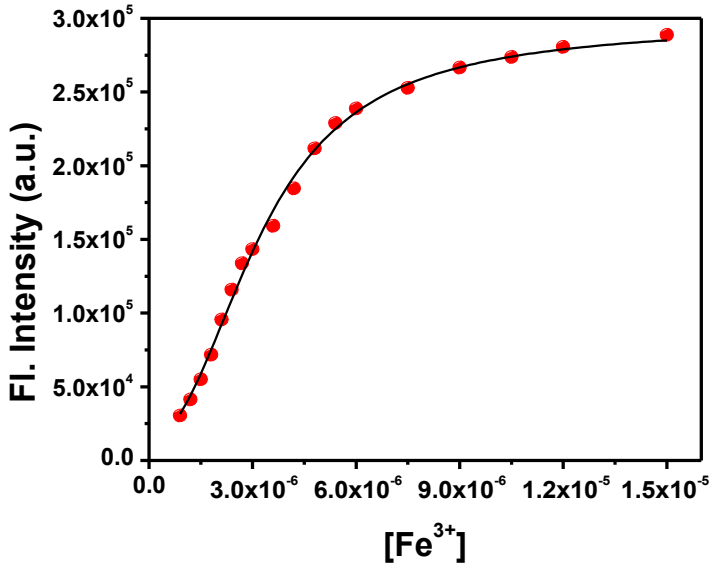

Fig. S33 Non-linear curve fitting (I_{590} vs. conc. of Fe^{3+}, λ_{exc} = 410 nm) for the determination of association constant of PYTG with Fe^{3+}.

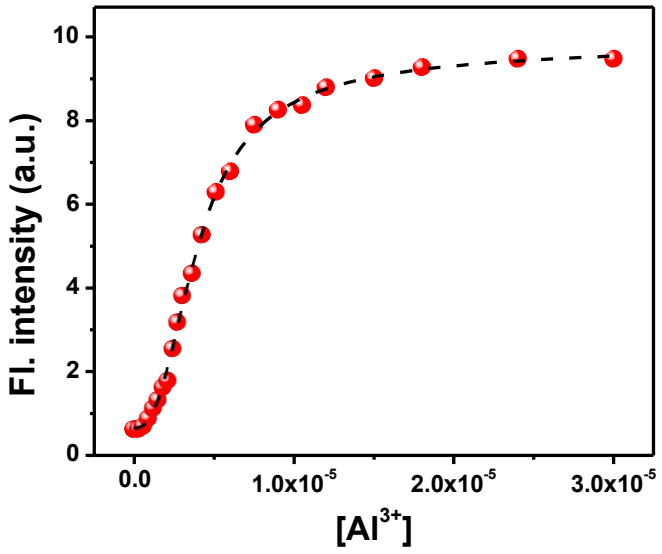

Fig. S34 Non-linear curve fitting (I_{590} vs. conc. of Al^{3+}, λ_{exc} = 410 nm) for the determination of association constant of PYTG with Al^{3+}.

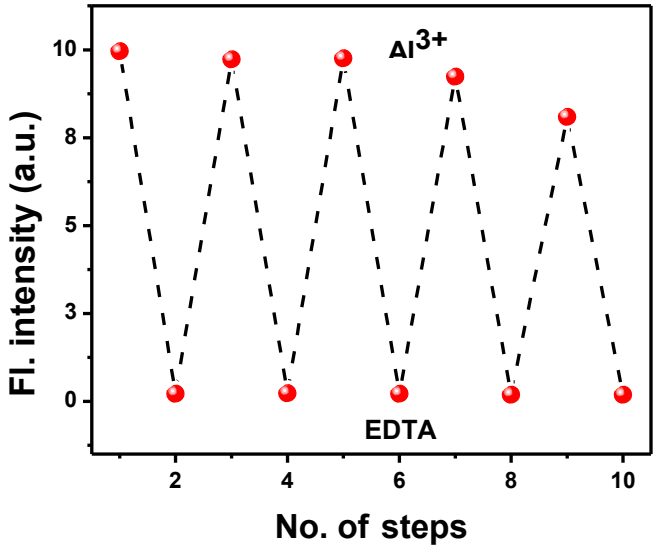

Fig. S35 Fluorescence (at 590 nm, λ_{exc} = 410 nm) on-off switching cycles of PYTG (3 μM, MeCN:H_2O; 3:2, v/v) using Al^{3+} (10 eqv.) and ethylenediaminetetraacetic acid (EDTA, 10 eqv.), respectively.

Static excimer formation:

Lifetime measurements of PYTG (3 μM in semi-aqueous medium, MeCN:H_2O; 3:2, v/v) in the presence of Fe^{3+} and Al^{3+} ions were carried out exciting by a 408 nm diode laser and monitoring at monomer (λ_{em} = 470 nm) and excimer (λ_{em} = 590 nm) emission bands (Fig. S36 and S37). The amplitude average decay time was increased upon addition of metal ions while monitoring the decay at the excimer emission band. After addition of excess metal ions (> 3 eqv.), the amplitude average decay time was found to be constant (Fig. S36). No such variation of decay time was observed while monitoring the decay at monomer emission band (Fig. S37). These results indicate the formation of the static excimer (Table S5).

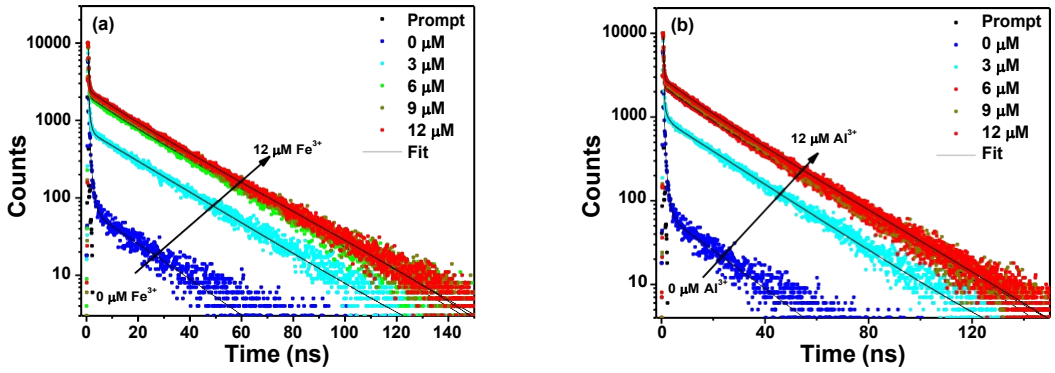

Fig. S36 Fluorescence decay profiles (λ_{exc} = 408 nm, λ_{em} = 590 nm) of PYTG (3 μM) with increasing concentration of (a) Fe^{3+} and (b) Al^{3+} ions in semi-aqueous medium (MeCN:H_2O, 3:2, v/v). The continuous black line indicates fit to the decay curves.

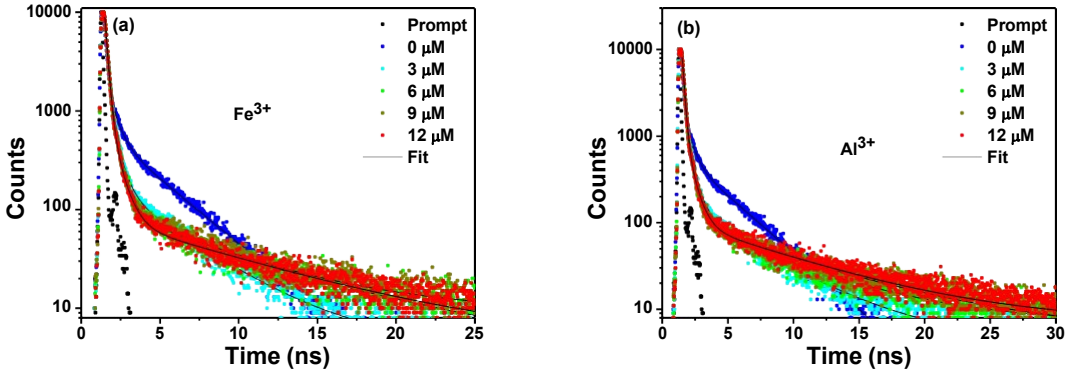

Fig. S37 Fluorescence decay profiles (λ_{exc} = 408 nm, λ_{em} = 470 nm) of PYTG (3 μM) with increasing concentration of (a) Fe^{3+} and (b) Al^{3+} ions in semi-aqueous medium (MeCN:H_2O, 3:2, v/v). The continuous black line indicates fit to the decay curves.

Table S5 Fluorescence decay parameters (λ_{exc} = 408 nm) of PYTG (3 μM) in semi-aqueous medium (MeCN:H_2O, 3:2, v/v) with varying concentration of Fe^{3+} and Al^{3+} ions; the decay times (τ_1, τ_2, and τ_3) and the respective fractional contributions (α_1, α_2 and α_3), the weighted average decay (τ_{av}) and the quality of fitting (χ^2) are shown. The respective emission wavelengths (nm) were indicated (λ_{exc} = 408 nm).

Metal ions	λ_{exc} = 408 nm	Decay parameters									
	Concentration (μM)	$\tau_1(\alpha_1)$		$\tau_2(\alpha_2)$		$\tau_3(\alpha_3)$		$\tau_{avg.}$		χ^2	
		470	590	470	590	470	590	470	590	470	590
Fe^{3+}	0	0.1 (16.5)	0.2 (25.1)	0.6 (23.5)	0.8 (49.6)	3.4 (59.9)	17.3 (25.26)	1.7	4.8	1.07	1.11
	3	0.1 (26.7)	0.4 (3.1)	0.5 (28.7)	8.6 (6.6)	3.3 (44.6)	22.9 (90.3)	1.6	21.3	1.16	1.13
	6	0.2 (44.5)	0.3 (4.0)	0.6 (29.3)	7.9 (6.9)	5.5 (24.3)	23.2 (89.1)	1.6	21.2	1.20	1.14
	9	0.2 (44.6)	0.2 (5.2)	0.6 (25.4)	3.3 (3.2)	9.1 (30.0)	22.5 (91.6)	2.9	20.5	1.18	1.11
	12	0.2 (41.8)	0.2 (4.6)	0.6 (27.0)	1.5 (2.5)	10.4 (31.17)	22.3 (92.9)	3.5	20.6	1.09	1.09
Al^{3+}	0	0.1 (16.5)	0.2 (25.1)	0.6 (23.5)	0.8 (49.6)	3.4 (59.9)	17.3 (25.3)	1.7	4.8	1.07	1.11
	3	0.1 (42.9)	0.2 (19.6)	0.5 (26.9)	0.8 (14.1)	3.6 (30.2)	21.3 (66.3)	2.8	14.3	1.18	1.08
	6	0.2 (62.8)	0.2 (3.2)	0.6 (16.1)	5.9 (4.1)	8.7 (21.1)	22.7 (92.7)	2.1	21.3	1.19	1.12
	9	0.2 (53.3)	0.2 (2.9)	0.6 (21.4)	12.9 (16.6)	9.4 (25.3)	24.4 (80.5)	2.6	21.8	1.25	1.15
	12	0.2 (41.7)	0.2 (4.2)	0.6 (23.2)	7.9 (5.4)	11.6 (35.1)	22.9 (90.4)	4.3	21.1	1.31	1.10

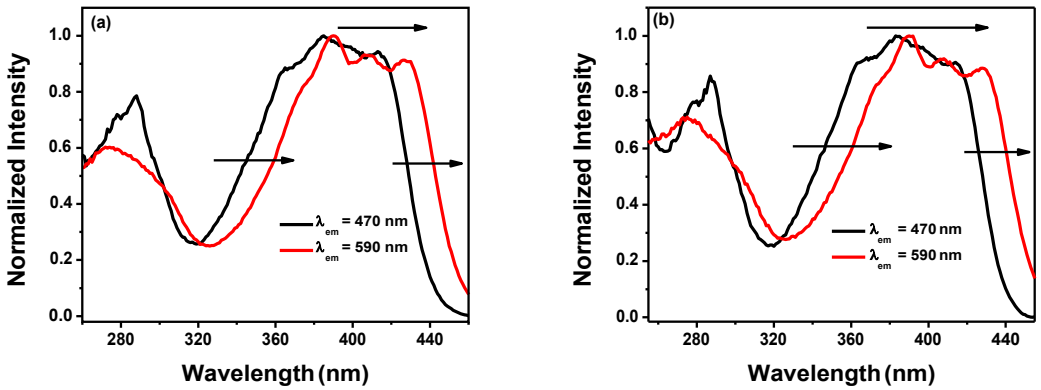

Fig. S38 Normalized excitation spectra of PYTG (3 μM, MeCN:H_2O, 3:2, v/v) monitoring at the monomer (λ_{em}= 470 nm) and excimer (λ_{em}= 590 nm) emission peaks in the presence of (a) Fe^{3+} and (b) Al^{3+} ions.

The formation of static excimer was also probed by excitation spectra for both the emission bands of PYTG in the presence of Fe^{3+} and Al^{3+} ions. A broad and red-shifted excitation profile was observed for the excimer emission as compared to that of the monomer emission (Fig. S38). This result is a clear indication of static excimer formation in the presence of trivalent metal ions Fe^{3+} and Al^{3+}.

XII. Computational investigations

Ground state geometry optimizations of PYTG were carried out using the Gaussian 09 program package. The molecular structure obtained through AM1 energy minimization in Materials studio 6.1 was taken as the input geometry and was optimized at the B3LYP/6-31G(d,p) level.

We observed that the HOMO of PYTG distributed from one pyrene to another through imine bond. The dihedral angles of three pyrene units with respect to the central triaminoguanidinium core are -31°, -28° and -22°. The two dihedral angles are similar in comparison to the third one which could be a reason for the molecular electronic distribution only over two pyrene units attached to triaminoguanidinium core.[35] Thomas C. W. Mak and co-workers reported a C_3-symmetric Schiff-base probe for Zn^{2+} sensing. They also observed similar HOMO distribution in the C_3-symmetric molecular fluorescent probe.[36] To know more about the orbital contribution, we have further carried out time-dependent density functional theory (TD-DFT, spin unrestricted) calculation using Gaussian 09 programme package and analysed the electronic transitions.[37] The molecular orbital of PYTG displayed both alpha (α) and beta (β) spin states.[38] The HOMO-1 (β) of PYTG have homogeneous electron density distribution over three pyrene units (Fig. S39). The main transitions occurred from HOMO-1 to LUMO and HOMO-1 to LUMO+1 (both α and β spin orbitals) and their contributions to the lowest energy excitations were 49% and 41%, respectively. The probable electronic transitions and oscillator strengths of PYTG based on the TD-DFT calculations are tabulated in Table S6.

Table S6 The salient features of the most probable electronic transitions with oscillator strengths obtained from the TD-DFT calculation.

Excitation energy (nm)	**Oscillator strength (f)**	**Electronic transition**	**Percentage (%)**
493.19	0.445	HOMO-1 (α) to LUMO (α)	49
		HOMO-1 (β) to LUMO (β)	49
411.62	0.162	HOMO-1 (α) to LUMO+1 (α)	41
		HOMO (α) to LUMO+2 (α)	7
		HOMO-1 (β) to LUMO+1 (β)	41
		HOMO (β) to LUMO+2 (β)	7
402.17	0.158	HOMO-1 (α) to LUMO+2 (α)	47
		HOMO-1 (β) to LUMO+2 (β)	47

MOs	α-spin orbital	β-spin orbital
LUMO+2 α = -1.25 eV β = -1.72 eV	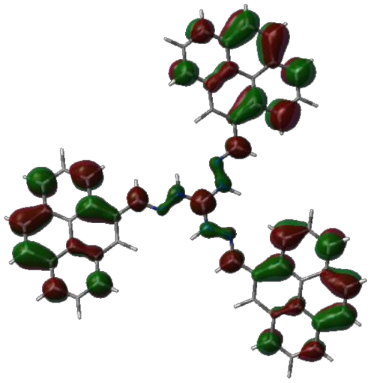	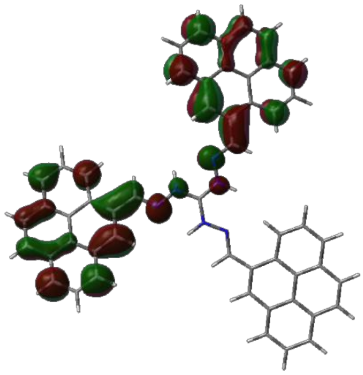
LUMO+1 α = -2.02 eV β = -1.75 eV	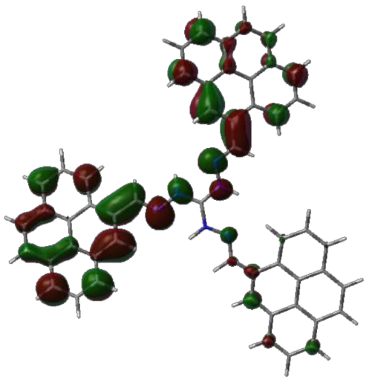	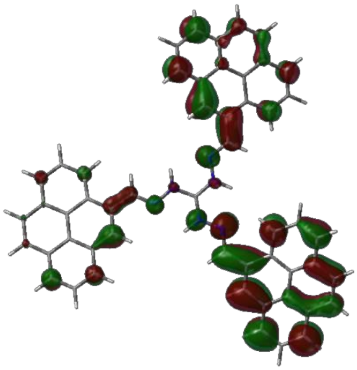
LUMO α = -2.04 eV β = -2.04 eV	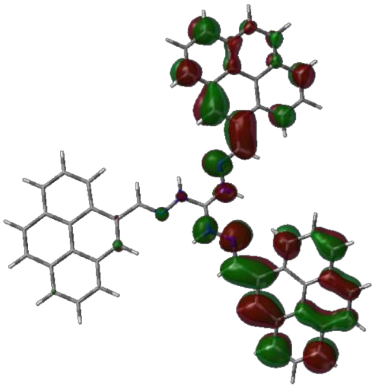	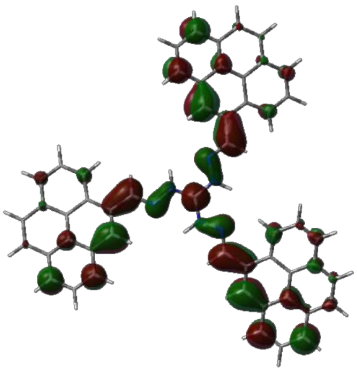

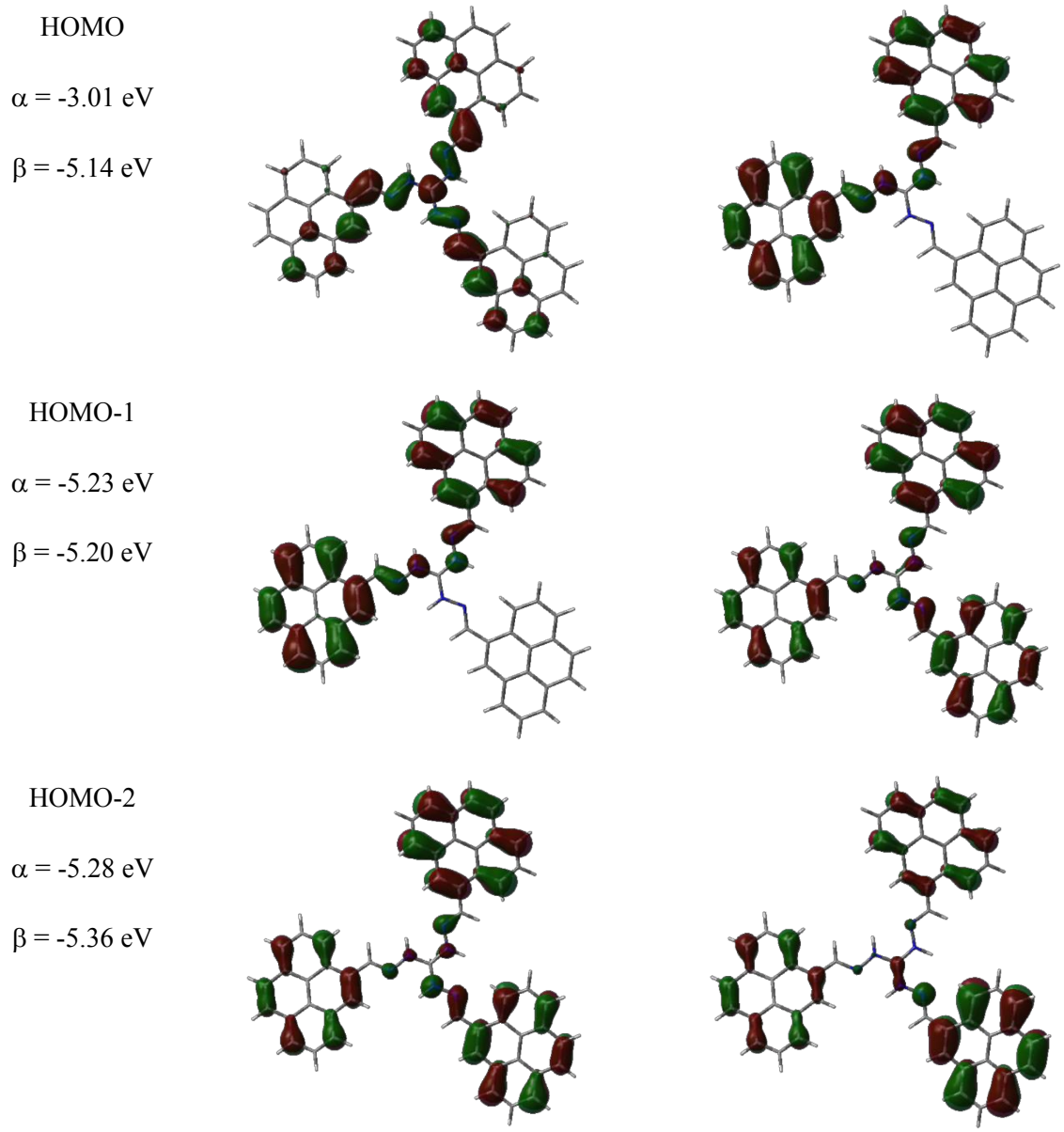

Fig. S39 The optimized ground-state HOMO-2, HOMO-1, HOMO, LUMO, LUMO+1 and LUMO +2 distributions (spin unrestricted) and the respective energy values (eV) of β ,α spin orbitals of PYTG obtained by density functional theory (DFT) calculations at the B3LYP/6-31G(d,p) level.

XII. Electrochemical measurement

The experimental HOMO/LUMO energy levels of PYTG in DCM were evaluated by cyclic voltammetry (CV) experiment. PYTG show reversible oxidation and reduction processes, indicative of good electrochemical stability. CV experiments were conducted at room temperature using degassed DCM solutions of PYTG (concentration: 1×10^{-3} M) containing 0.1 M n-Bu_4PF_6 as a supporting electrolyte in a three-electrode electrochemical cell (scan rate: 100 mV/s). Glassy carbon, $Ag/AgNO_3$ (1 M $AgNO_3$) electrode and Pt wire were used respectively, as a working, reference and counter electrode. The HOMO and LUMO energy levels of PYTG was calculated by the following equations using the onset potentials corrected against the Fc/Fc^+ (Fc = ferrocene) couple: $E_{HOMO} = -(4.8 + {}^{ox}E_{onset}$ vs. $Fc/Fc^+)$ eV; $E_{LUMO} = -(4.8 + {}^{red}E_{onset}$ vs. $Fc/Fc^+)$ eV. HOMO-LUMO energy levels were found to be −5.73 and −3.48 eV, respectively analogous to that obtained from the DFT calculations (β spin state, Fig. S40).

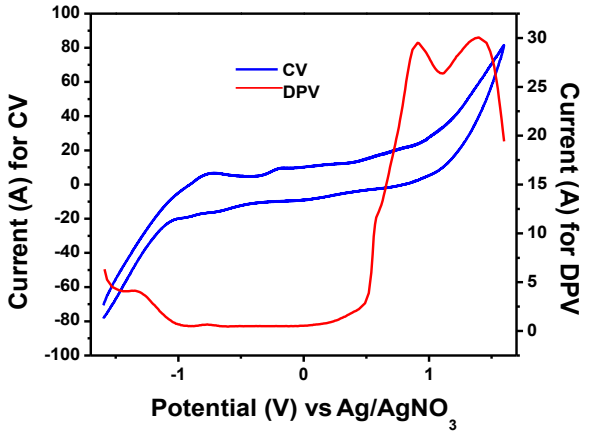

Fig. S40 Cyclic voltammogram and differential pulse voltammogram of PYTG (1 mM) in DCM vs Ag/Ag^+ at 100 mV/s scan rate.

XIV. Comparative table

Table S7 A comparative account of multifunctional applications of PYTG in view of single component white light emission, fluorescent molecular switch in the presence of metal ions (particularly Fe^{3+}/Al^{3+}) through the probing of dynamic and static excimer formation with other notable molecular optical materials.

Sl. No.	System	Probing the excimer formation		Single component WLE (CIE)	Selective detection of analytes (LOD)	Reference
		Dynamic	*Static*			
1	PYTG	Yes Concentration and temperature effect (Stevens-Ban plot)	Yes Chelation-enhanced fluorescence	Solution: (0.33, 0.34) Thin film: (0.33, 0.38)	Fe^{3+} (5.4 nM), Al^{3+} (14 nM)	Present work
Single component white light emission						
2	CIBDBT	--	--	(0.33, 0.35)	--	*Nat. Commun.*, 2017, **8**, 416.[39]
3	CPzPO	--	--	(0.31, 0.32)	--	*Adv. Funct. Mater.*, 2017, **27**, 1703918.[40]
4	TPE-Pys	--	--	(0.30,0.41)	--	*Chem. Sci.*, 2018: DOI: 10.1039/c8sc01709c.[41]
5	SDB_2t	--	--	(0.27, 0.27)	--	*Chem. Sci.*, 2017, **8**, 1909.[42]
6	Cz^9PhAn	--	--	(0.30, 0.33)	--	*Chem. Sci.*, 2016, **7**, 3556.[43]
7	SCP	--	--	(0.27, 0.29)	--	*Chem. Sci.*, 2016, **7**, 2201.[44]
8	Probe-1	--	--	(0.32, 0.38)	--	*Chem. Commun.*, 2017, **53**, 9269.[45]
9	Probe-1	--	--	(0.357, 0.339)	--	*Chem. Commun.*, 2017, **53**, 7832.[46]
10	L-Cl.ClO_4	--	--	(0.32, 0.33)	--	*Chem. Commun.*, 2014, **50**, 15878.[47]

11	PQCz-T	--	--	(0.36, 0.28)	--	*Chem. Commun.*, 2018, **54**, 1786.[48]
12	BTImP	--	--	(0.30, 0.35)	--	*J. Mater. Chem. C*, 2016, **4**, 2011.[49]
13	BPTP	--	--	(0.29, 0.23)	--	*J. Mater. Chem. C*, 2015, **3**, 4563.[50]
14	Probe-1	--	--	(0.33, 0.30)	--	*J. Phys. Chem. C,* 2017, **121**, 5277.[51]
15	3-DPH-XO	--	--	(0.27,0.35)	--	*J. Phys. Chem. Lett.,* 2017, **8**, 4808.[52]
16	Probe-10	--	--	(0.33, 0.33)	--	*J. Phys. Chem. C,* 2016, **120**, 26986.[53]
17	PyBPNMe2	--	--	(0.31, 0.34)	--	*J. Phys. Chem. A,* 2016, **120**, 5838.[54]
Excimer formation and detection of metal ions						
18	Probe-1	Concentration effect	Chelation	--	Al^{3+} (0.51 μM)	*Org. Lett*., 2012, **14**, 3420.[55]
19	Probe-1	Concentration effect	Chelation	--	Cd^{2+} (NA), Ca^{2+} (NA), Cu^{2+} (NA)	*Org. Lett.,* 2001, **3**, 889.[56]
20	Probe-L	Concentration effect	Chelation	--	Zn^{2+} (NA)	*J. Phys. Chem. B,* 2007, **111**, 8812.[57]
21	Probe-L	Concentration effect	Chelation	--	Sn^{2+} (25.7 nM)	*Dalton Trans*., 2015, **44**, 14388.[22]
22	Probe- (S)-1	Concentration effect	Chelation	--	Cu^{2+} (NA)	*Tetrahedron Lett.,* 2006, **47,** 4577.[58]
23	Probe-1	--	Chelation	--	Cu^{2+} (NA)	*Org. Lett.,* 2008, **10,** 1963.[59]
24	Probe-4	--	Chelation	--	Cu^{2+} (1 μM)	*Org. Lett.,* 2009, **11**, 3378.[60]
25	CP-1	--	Chelation	--	Ca^{2+} (NA)	*Org. Lett.,* 2002, **4**, 683.[61]
26	Probe-L	--	Chelation	--	Cu^{2+} (NA), Ag+ (NA), Zn^{2+} (NA)	*Inorg. Chem.,* 2013, **52**, 121.[62]

27	Probe-1	--	Chelation	--	Cu^{2+} (NA), Hg^{2+} (NA)	*Tetrahedron Lett*., 2011, **52**, 1938.[63]
28	MAB	--	Chelation	--	Cu^{2+} (NA)	*Tetrahedron Lett.,* 2015*,* **56**, 162.[64]
29	Probe-1	Concentration effect	--	--	Cu^{2+} (40 nM)	*J. Org. Chem.,* 2007, **72**, 5980.[65]
Detection of trivalent metal ions						
30	Py-TPE	--	--	--	Al^{3+} (NA), Fe^{3+} (NA), Cr^{3+} (NA)	*Chem. Commun.*, 2013, **49**, 1503.[66]
31	Ligand 1	--	--	--	Al^{3+} (0.2 μM), Fe^{3+} (0.3 μM), Cr^{3+} (0.5 μM)	*Chem. Commun.*, 2012, **48**, 3000.[67]
32	SBPQ	--	--	--	Al^{3+} (32.4 nM), Fe^{3+} (NA), Cr^{3+} (NA)	*Chem. Commun.*, 2013, **49**, 10739.[68]
33	5	--	--	--	Al^{3+} (0.5 μM), Fe^{3+} (NA), Cr^{3+} (0.2 μM)	*Chem. Commun.*, 2014, **50**, 12258.[69]
34	PCS1	--	--	--	Al^{3+} (2.4 μM), Fe^{3+} (1 μM), Cr^{3+} (1 μM)	*J. Mater. Chem. C*, 2016, **4**, 2056.[70]
35	RND	--	--	--	Al^{3+} (1.74 nM), Fe^{3+} (2.90 μM), Cr^{3+} (2.36 μM)	*Dalton Trans.*, 2015, **44**, 11805.[71]
36	Probe-3	--	--	--	Al^{3+}, Fe^{3+}, Cr^{3+}, Ga^{3+}, Hg^{2+} (all under 1 μM)	*Dalton Trans.*, 2016, **45**, 9513.[72]

[#]NA: not available

XV. NMR and mass spectra

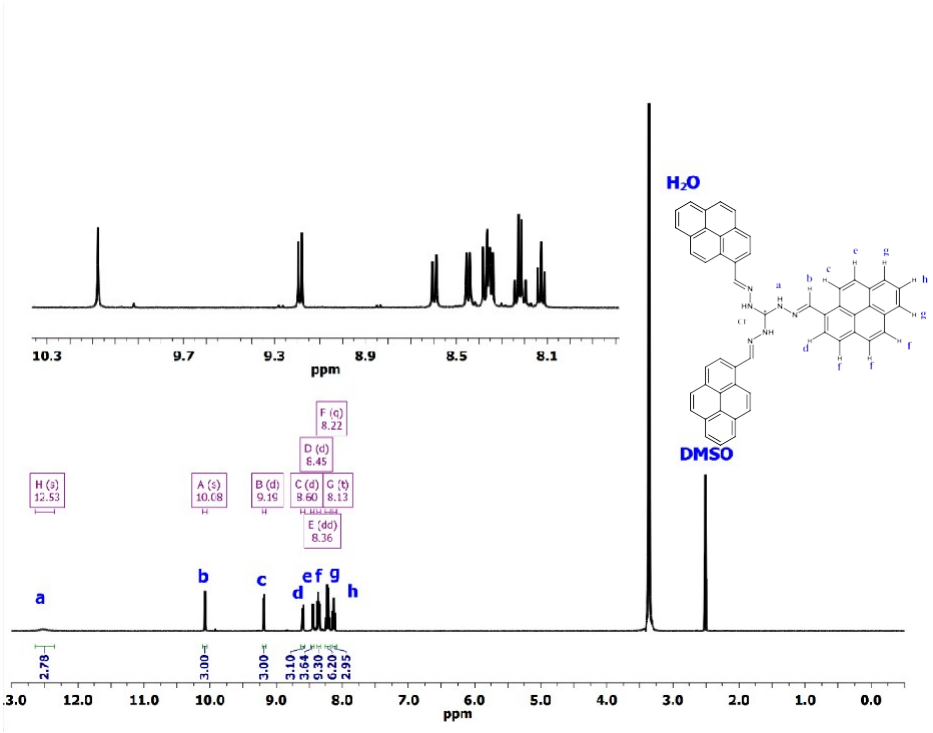

Fig. S41 ^{1}H NMR spectrum of PYTG in DMSO-d_6 at room temperature.

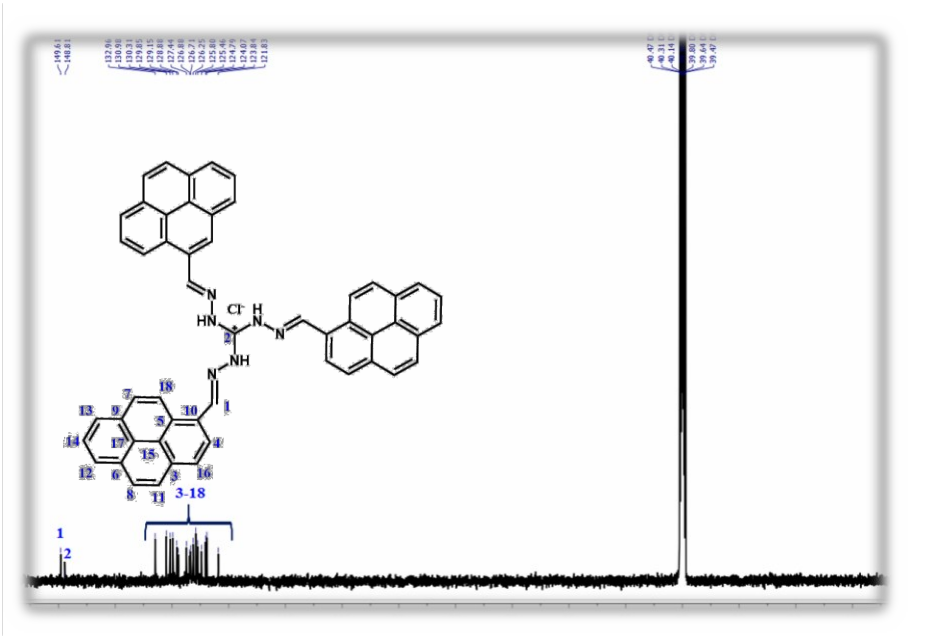

Fig. S42 ^{13}C NMR spectrum of PYTG in DMSO-d_6 at room temperature.

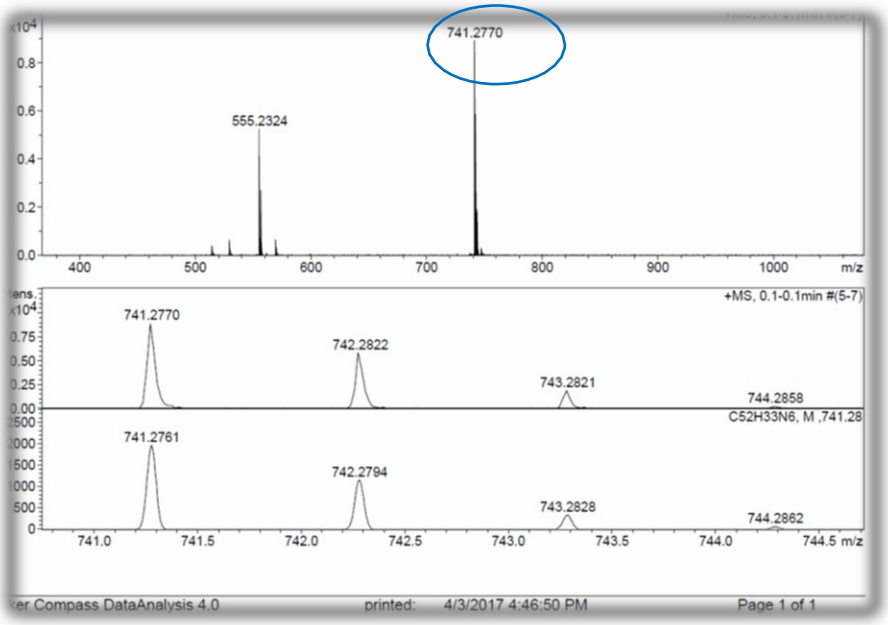

Fig. S43 HRMS-ESI mass spectrum of PYTG.

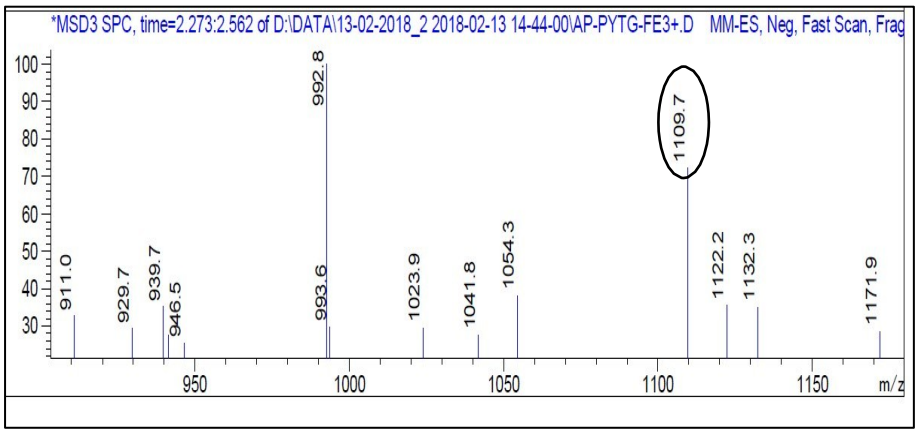

Fig. S44 LCMS-ESI mass spectrum of PYTG with Fe^{3+}.

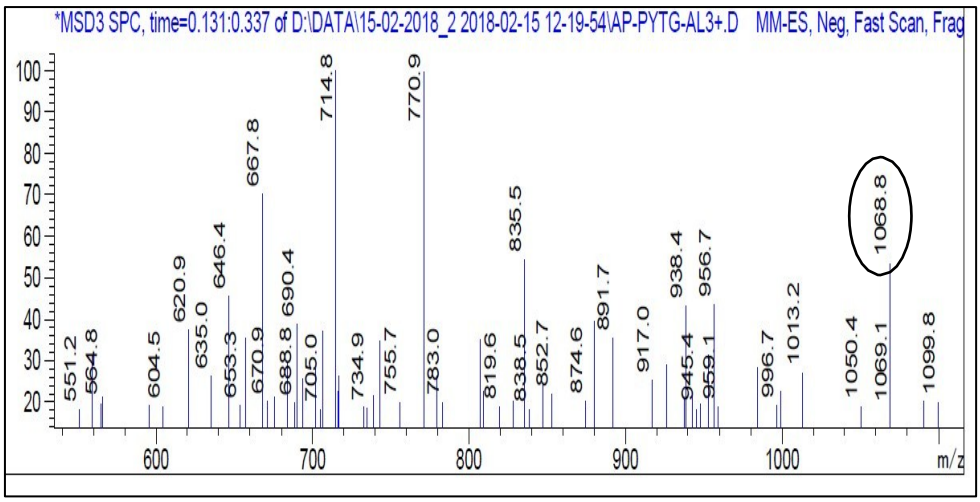

Fig. S45 LCMS-ESI mass spectrum of PYTG with Al^{3+}.

XVI. Input geometry of PYTG

Ground state optimization:

```
%nprocshared=16
%mem=6GB
%chk=vk.chk
# opt ub3lyp/6-31g(d,p) guess=mix geom=connectivity

vk

0 2
 N                 -1.32736100    0.32816100   -0.01631100
 C                 -0.05337800   -0.11855300   -0.00074900
 N                  0.96896300    0.76469200   -0.00028500
 N                  0.19238500   -1.44635300    0.01498100
 N                 -2.36044900   -0.55026200   -0.00603400
 N                  1.46693300   -1.91366300    0.07179600
 N                  0.71783100    2.09760600    0.00979800
 C                 -3.56030600   -0.03677900   -0.07124500
 C                  1.59704100   -3.20980800   -0.01244800
 C                  1.75501300    2.88671600   -0.08072200
 C                 -6.27741300    1.12060900   -0.45420400
 C                 -6.07500700   -0.24914000   -0.21527900
 C                 -7.23050200   -1.09662500   -0.14926300
 C                 -8.53851400   -0.53866900   -0.30961800
 C                 -8.67905300    0.83938700   -0.53545500
 C                 -7.55679400    1.65461400   -0.60887700
 C                 -7.09634000   -2.50136100    0.07070400
 C                 -8.24830300   -3.34125900    0.13399700
 C                 -9.54438100   -2.74485300   -0.02679600
 C                 -9.68052200   -1.40773100   -0.23845400
 C                 -4.75508600   -0.85282400   -0.03789100
 C                 -4.66054100   -2.21754100    0.17105100
 C                 -5.79452000   -3.07153300    0.22847100
 C                 -5.67823600   -4.45920000    0.44421900
 C                 -6.80883100   -5.26862700    0.50288600
 C                 -8.08195600   -4.72057000    0.35025200
 C                  4.04726000    4.68398800   -0.69000900
 C                  2.79058100    5.18087100   -0.30537900
 C                  2.63444800    6.60250100   -0.19774200
 C                  3.74524200    7.46659900   -0.45687700
 C                  4.98187000    6.91173600   -0.82138300
 C                  5.12415700    5.53494100   -0.93939400
 C                  1.37574000    7.17525100    0.15872400
 C                  1.22400100    8.59040300    0.26256300
 C                  2.36255800    9.42540300    0.00157200
 C                  3.56426700    8.88733400   -0.34153400
 C                  1.63745400    4.32838200   -0.02178800
 C                  0.43129400    4.91522600    0.31719600
 C                  0.25670600    6.32226900    0.41365700
```

C	-0.97833500	6.90234100	0.76506600
C	-1.11477900	8.28399500	0.86225500
C	-0.02876300	9.12287600	0.61454300
C	4.40552600	-2.07551700	0.58307800
C	4.16434500	-3.42147700	0.26718200
C	5.28735200	-4.31287600	0.20207800
C	6.60941700	-3.81289000	0.42453100
C	6.79286500	-2.45261900	0.72092400
C	5.69988100	-1.60158200	0.80695400
C	5.11182000	-5.70370000	-0.07323400
C	6.23388600	-6.58263200	-0.13626400
C	7.54569100	-6.04099500	0.07875000
C	7.72171400	-4.71879500	0.34751200
C	2.82911300	-3.96539900	0.01807200
C	2.69704000	-5.32439600	-0.22465600
C	3.79651300	-6.22231800	-0.27960000
C	3.63260400	-7.59680000	-0.54024800
C	4.73488800	-8.44469200	-0.59984900
C	6.02234200	-7.94761100	-0.40173100
H	-1.45161800	1.33991000	-0.05358000
H	1.91019900	0.37690200	-0.05350900
H	-0.62329600	-2.05685600	-0.03560100
H	-3.66572400	1.04821200	-0.14133400
H	0.69335400	-3.81909800	-0.14227500
H	2.74879900	2.44438100	-0.18392100
H	-5.43303700	1.79653500	-0.53093600
H	-9.67431400	1.25981500	-0.65666000
H	-7.67104400	2.71986500	-0.79100100
H	-10.41994400	-3.38775600	0.02314200
H	-10.66716300	-0.96713100	-0.36056100
H	-3.67748800	-2.65669300	0.30995500
H	-4.68850300	-4.89260900	0.56587900
H	-6.69875800	-6.33692400	0.66971500
H	-8.96117700	-5.35827000	0.39749600
H	4.20242200	3.61776700	-0.81241400
H	5.82367400	7.57135700	-1.01687400
H	6.08108300	5.11158100	-1.23267800
H	2.24352100	10.50322900	0.08265500
H	4.41893600	9.52995400	-0.53919700
H	-0.41608000	4.27393200	0.53936000
H	-1.82843900	6.25360400	0.96155800
H	-2.07564400	8.71292000	1.13413300
H	-0.14197200	10.20133100	0.69233800
H	3.56670800	-1.39967900	0.66707300
H	7.79926000	-2.07772700	0.89105700
H	5.84886200	-0.55336500	1.05333000
H	8.39903000	-6.71282600	0.02661100
H	8.71912000	-4.31901900	0.51441000
H	1.70403700	-5.73345900	-0.40059800
H	2.63092800	-7.98957400	-0.69704900
H	4.59083300	-9.50257700	-0.80258000
H	6.87891100	-8.61542400	-0.44885900

TD-DFT calculation:

```
%nprocshared=16
%mem=6GB
%chk=vke.chk
# td=50-50 ub3lyp/6-31g(d,p) guess=mix geom=connectivity

vke

0 2
 N                 -1.32523438    0.33223478   -0.02169483
 C                 -0.05367447   -0.11996235   -0.00597701
 N                  0.97235799    0.75835205   -0.00743214
 N                  0.18594062   -1.44831991    0.01068376
 N                 -2.35966529   -0.54495232   -0.00942329
 N                  1.45969110   -1.91788035    0.07224072
 N                  0.72298492    2.09183797    0.00430546
 C                 -3.55911771   -0.03061206   -0.07471508
 C                  1.58860969   -3.21381684   -0.01711731
 C                  1.76046689    2.88020577   -0.08843512
 C                 -6.27359801    1.12610273   -0.46260320
 C                 -6.07280879   -0.24291373   -0.21862734
 C                 -7.22897673   -1.08888138   -0.14974909
 C                 -8.53632770   -0.53024257   -0.31194387
 C                 -8.67529859    0.84715109   -0.54244392
 C                 -7.55224370    1.66072601   -0.61889082
 C                 -7.09591289   -2.49294958    0.07473621
 C                 -8.24862260   -3.33141888    0.14065680
 C                 -9.54417509   -2.73431220   -0.02199314
 C                 -9.67915640   -1.39800037   -0.23787439
 C                 -4.75355198   -0.84707360   -0.03892987
 C                 -4.65976832   -2.21101113    0.17462021
 C                 -5.79464423   -3.06372964    0.23441338
 C                 -5.67980557   -4.45077036    0.45454616
 C                 -6.81112520   -5.25863193    0.51556934
 C                 -8.08358984   -4.71014469    0.36120288
 C                  4.04762520    4.67641837   -0.71004436
 C                  2.79406115    5.17384459   -0.31635529
 C                  2.63976255    6.59518553   -0.20535273
 C                  3.74954619    7.45877433   -0.46973910
 C                  4.98334693    6.90335926   -0.84271330
 C                  5.12350677    5.52681239   -0.96425183
 C                  1.38358610    7.16804144    0.15953611
 C                  1.23361665    8.58302971    0.26650018
 C                  2.37124570    9.41764526    0.00013190
 C                  3.57032544    8.87945766   -0.35091336
 C                  1.64228672    4.32174068   -0.02687318
 C                  0.43855489    4.90831770    0.32055467
 C                  0.26556949    6.31542323    0.41984383
 C                 -0.96681015    6.89593358    0.77953220
 C                 -1.10141831    8.27734888    0.87950481
```

C	-0.01658487	9.11584320	0.62671364
C	4.38826495	-2.08466094	0.62364528
C	4.15278533	-3.42595567	0.28463094
C	5.27801443	-4.31398845	0.21532719
C	6.59730626	-3.81439927	0.45367557
C	6.77542225	-2.45817158	0.77096394
C	5.67982769	-1.61146698	0.86337780
C	5.10701113	-5.70148067	-0.07878940
C	6.23128833	-6.57714069	-0.14542932
C	7.54057042	-6.03553265	0.08461474
C	7.71207211	-4.71682481	0.37161373
C	2.82079658	-3.96892354	0.01711087
C	2.69251335	-5.32513606	-0.24205257
C	3.79415280	-6.22020175	-0.29965754
C	3.63490111	-7.59179298	-0.57760535
C	4.73930357	-8.43631124	-0.64039602
C	6.02429885	-7.93921568	-0.42854075
H	-1.44236839	1.34382837	-0.05935822
H	1.90984687	0.36453528	-0.06298535
H	-0.63322481	-2.05243813	-0.04054832
H	-3.66590480	1.05368372	-0.14675824
H	0.68651091	-3.82258218	-0.15624379
H	2.75414245	2.43954238	-0.19528889
H	-5.42866795	1.80012610	-0.54206436
H	-9.66952284	1.26796156	-0.66492061
H	-7.66548298	2.72478655	-0.80477198
H	-10.41986479	-3.37581265	0.03001721
H	-10.66488524	-0.95726874	-0.36126649
H	-3.67738618	-2.64965785	0.31553175
H	-4.69114349	-4.88458076	0.57762952
H	-6.70212490	-6.32589099	0.68564256
H	-8.96291627	-5.34644565	0.41034315
H	4.20035244	3.61079170	-0.83574670
H	5.82403744	7.56218975	-1.04197704
H	6.07768834	5.10357271	-1.26421683
H	2.25362210	10.49480698	0.08365998
H	4.42369696	9.52153688	-0.55244796
H	-0.40679412	4.26693870	0.54747727
H	-1.81575338	6.24800313	0.98004873
H	-2.05978611	8.70629853	1.15758944
H	-0.12840902	10.19362115	0.70677748
H	3.54660341	-1.41384341	0.71388928
H	7.77919798	-2.08372388	0.95295873
H	5.82452946	-0.56764472	1.12749064
H	8.39521999	-6.70441158	0.02924285
H	8.70699768	-4.31756328	0.55007355
H	1.70204815	-5.73318294	-0.43061749
H	2.63569902	-7.98457067	-0.74527557
H	4.59886898	-9.49139876	-0.85646335
H	6.88207818	-8.60423548	-0.47822721

XVII. References

1. J. B. Birks, *Rep. Prog. Phys*., 1975, **38**, 903.
2. C. H. Lochmuller, A. S. Colborn, M. L. Hunnicutt and J. M. Harris, *J. Am. Chem. Soc.*, 1984, **106**, 4077.
3. K. Sekar and C. J. Claude, *Chem. Asian J.*, 2011, **6**, 964.
4. F. M. Winnik, *Chem. Rev.*, 1993, **93**, 587.
5. J. Hoche, H. C. Schmitt, A. Humeniuk, I. Fischer, R. Mitric and M. I. S. Rohr, *Phys. Chem. Chem. Phys.*, 2017, **19**, 25002.
6. J. S. Yang, C. S. Lin and C. Y. Hwang, *Org. Lett.*, 2001, **3**, 889.
7. K. S. Focsaneanu and J. C. Scaiano, *Photochem. & Photobiolo. Sciences*, 2005, **4**, 817.
8. T. M. F. Duarte and K. Müllen, *Chem. Rev.*, 2011, **111**, 7260.
9. G. K. Bains, S. H. Kim, E. J. Sorin and V. Narayanaswami, *Biochemistry*, 2012, **51**, 6207.
10. J. Y. Hu, Y. J. Pu, G. Nakata, S. Kawata, H. Sasabe and J. Kido, *Chem. Commun.*, 2012, **48**, 8434.
11. H. Garam, K. Dongwook, P. Younbong, B. Jean and K. Youngmi, *Angew. Chem. Int. Ed.*, 2015, **54**, 3912.
12. F. Xing, H. J. Yong, R. Carl and Y. Takehiko, *Chem. Eur. J.*, 2016, **22**, 11898.
13. S. Sarkar, S. Roy, A. Sikdar, R. N. Saha and S. S. Panja, *Analyst*, 2013, **138**, 7119.
14. C. Reichardt, *Chem. Rev*., 1994, **94**, 2319.
15. S. Kondo, Y. Taguchia and Y. Bie, *RSC Adv*., 2015, **5**, 5846.
16. C. Würth, M. Grabolle, J. Pauli, M. Spieles and U. R. Genger, *Nat. Protoc.*, 2013, **8**, 1535.
17. P. Avis and G. Porter, *J. Chem. Soc., Faraday Trans. 2: Mole. Chem. Phys.*, 1974, **70**, 1057.
18. M. S. Nicze, M. Wolszczak, J. Kroh and J. Mayer, *J. Photochem. Photobiol. A: Chemistry*, 1993, **75**, 125.
19. B. Bodenant, F. Fages and M. H. Delville, *J. Am. Chem. Soc.*, 1998, **120**, 7511.
20. C. Honda, Y. Katsumata, R. Yasutome, S. Yamazaki, S. Ishii, K. Matsuoka and K. Endo, *J. Photochem. Photobiol. A: Chemistry*, 2006, **182**, 151.
21. M. Shellaiah, Y. H. Wu, A. Singh, M. V. R. Raju and H. C. Lin, *J. Mater. Chem. A*, 2013, **1**, 1310.
22. S. Adhikari, S. Mandal, A. Ghosh, S. Guria and D. Das, *Dalton Trans.*, 2015, **44**, 14388.
23. C. T. Yeh and C. Y. Chen, *RSC Adv.*, 2017, **7**, 6023.
24. M. Zhao, X. Zhou, J. Tang, Z. Deng, X. Xu, Z. Chen, X. Li, L. Yang and L. J. Ma, *Spectrochim. Acta, Part A*, 2017, **173**, 235.
25. J. S. Melo, J. Pina, F. Pina, C. Lodeiro, A. J. Parola, J. C. Lima, M. T. Albelda, M. P. Clares, E. G. Espana, *J. Phys. Chem. A*, 2003, **107**, 11307.
26. X. Gong, S. Wang, D. Moses, G. C. Bazan and A. J. Hegger, *Adv. Mater.*, 2005, **17**, 2053.
27. G. M. Farinola and R. Ragni, *Chem. Soc. Rev.*, 2011, **40**, 3467.
28. C. Yuanjing, S. Tao, Y. Jiancan, Y. Yu, W. Zhiyu and Q. Guodong, *Adv. Funct. Mater.*, 2015, **25**, 4796.

29. C. S. McCamy, *Color Res. Appl.*, 1992, **17**, 142.

30. B. Pramanik and D. Das, *J. Phys. Chem. C*, 2018, **122**, 3655.

31. N. Saadati, M. P. Abdullah, Z. Zakaria, S. B. T. Sany, M. Rezayi and H. Hassonizadeh, *Chem. Cent. J.*, 2013, **7**, 63.

32. J. S. Renny, L. L. Tomasevich, E. H. Tallmadge and D. B. Collum, *Angew. Chem. Int. Ed.*, 2013, **52**, 11998.

33. B. Valeur, Molecular Fluorescence: Principles and Applications, Wiley-VCH, Weinheim, 2001.

34. X. J. Jiang, M. Li, H. L. Lu, L. H. Xu, H. Xu, S. Q. Zang, M. S. Tang, H. W. Hou and T. C. W. Mak, *Inorg. Chem.*, 2014, **53**, 12665.

35. Y. Wan, J. Li, X. Peng, C. Huang, Q. Qi, W. -Y. Lai and W. Huang, *RSC Adv*., 2017, **7**, 35543.

36. Y. Zhou, Z. Li, S. Zang, Y. Zhu, H. Zhang, H. Hou and T. C. W. Mak, *Org. Lett*., 2012, **14**, 1214.

37. Y. Gao, C. Liu and Y. Jiang, *J. Phys. Chem. A*, 2002, **106**, 5380.

38. F. Chen, G. Liu, Y. Shi, P. Xi, J. Cheng, J. Hong, R. Shen, X. Yao, D. Bai and Z. Zeng, *Talanta*, 2014, **124**, 139.

39. Z. He, W. Zhao, J. W. Y. Lam, Q. Peng, H. Ma, G. Liang, Z. Shuai and B. Z. Tang, *Nat. Commun.*, 2017, **8**, 416.

40. X. Zongliang, H. Qiuyi, Y. Tao, W. Leyu, M. Zhu, L. Wenlang, Y. Zhan, Z. Yi, L. Siwei, X. Jiarui, C. Zhenguo and P. A. Matthew, *Adv. Funct. Mater.*, 2017, **27**, 1703918.

41. X. Feng, C. Qi, H. T. Feng, Z. Zhao, H. H. Y. Sung, I. D. Williams, R. T. K. Kwok, J. Y. Lam, A. Qin and B. Z. Tang, *Chem. Sci.*, 2018, DOI: 10.1039/c8sc01709c.

42. B. Xu, H. Wu, J. Chen, Z. Yang, Z. Yang, Y. C. Wu, Y. Zhang, C. Jin, P.Y. Lu, Z. Chi, S. Liu, J. Xu and M. Aldred, *Chem. Sci.*, 2017, **8**, 1909.

43. Y. H. Chen, K. C. Tang, Y. T. Chen, J. Y. Shen, Y. S. Wu, S. H. Liu, C. S. Lee, C. H. Chen, T. Y. Lai, S. H. Tung, R. J. Jeng, W. Y. Hung, M. Jiao, C. C. Wu and P. T. Chou, *Chem. Sci.*, 2016, **7**, 3556.

44. B. Xu, Y. Mu, Z. Mao, Z. Xie, H. Wu, Y. Zhang, C. Jin, Z. Chi, S. Liu, J. Xu, Y. C. Wu, P. Y. Lu, A. Lien and M. R. Bryce, *Chem. Sci.*, 2016, **7**, 2201.

45. N. N. Zhang, C. Sun, X. M. Jiang, X. S. Xing, Y. Yan, L. Z. Cai, M. S. Wang and G. C. Guo, *Chem. Commun.*, 2017, **53**, 9269.

46. H. Liu, X. Cheng, H. Zhang, Y. Wang, H. Zhang and S. Yamaguchi, *Chem. Commun.*, 2017, **53**, 7832.

47. X. H. Jin, C. Chen, C. X. Ren, L. X. Cai and J. Zhang, *Chem. Commun.*, 2014, **50**, 15878.

48. B. Sk, S. Khodia and A. Patra, *Chem. Commun.*, 2018, **54**, 1786.

49. K. Sakai, S. Tsuchiya, T. Kikuchi and T. Akutagawa, *J. Mater. Chem. C*, 2016, **4**, 2011.

50. C. Chen, X. H. Jin, X. J. Zhou, L. X. Cai, Y. J. Zhang and J. Zhang, *J. Mater. Chem. C*, 2015, **3**, 4563.

51. I. E. Serdiuk, *J. Phys. Chem. C*, 2017, **121**, 5277.

52. Y. Zhang, Y. Miao, X. Song, Y. Gao, Z. Zhang, K. Ye and Y. Wang, *J. Phys. Chem. Lett.*, 2017, **8**, 4808.

53. S. Achelle, J. R. López, C. Katan and F. R. Guen, *J. Phys. Chem. C*, 2016, **120**, 26986.

54. A. K. Pati, S. J. Gharpure and A. K. Mishra, *J. Phys. Chem. A*, 2016, **120**, 5838.

55. X. Sun, Y. W. Wang and Y. Peng, *Org. Lett.*, 2012, **14**, 3420.

56. J. S. Yang, C. S. Lin and C. Y. Hwang, *Org. Lett.*, 2001, **3**, 889.

57. Y. Shiraishi, K. Ishizumi, G. Nishimura and T. Hirai, *J. Phys. Chem. B*, 2007, **111**, 8812.

58. E. J. Jun, H. N. Won, J. S. Kim, K. H. Lee and J. Yoon, *Tetrahedron Lett.*, 2006, **47**, 4577.

59. H. J. Kim, J. Hong, A. Hong, S. Ham, J. H. Lee and J. S. Kim, *Org. Lett.*, 2008, **10**, 1963.

60. H. S. Jung, M. Park, D. Y. Han, E. Kim, C. Lee, S. Ham and J. S. Kim, *Org. Lett.*, 2009, **11**, 3378.

61. J. Strauss and J. Daub, *Org. Lett.*, 2002, **4**, 683.

62. J. F. Lodeiro, C. Núñez, C. S. Castro, E. Bértolo, J. S. S. Melo, J. L. Capelo and C. Lodeiro, *Inorg. Chem.*, 2013, **52**, 121.

63. V. Chandrasekhar and M. D. Pandey, *Tetrahedron Lett*., 2011, **52**, 1938.

64. S. Malkondu, D. Turhan and A. Kocak, *Tetrahedron Lett.*, 2015, **56**, 162.

65. J. Xie, M. Ménand, S. Maisonneuve and R. Métivier, *J. Org. Chem.*, 2007, **72**, 5980.

66. X. Chen, X. Y. Shen, E. Guan, Y. Liu, A. Qin, J. Z. Sun and B. Z. Tang, *Chem. Commun.*, 2013, **49**, 1503.

67. A. B. Bon, A. M. Costero, S. Gil, M. Parra, J. Soto, R. M. Manez and F. Sancenon, *Chem. Commun.*, 2012, **48**, 3000.

68. S. Goswami, K. Aich, S. Das, A. K. Das, D. Sarkar, S. Panja, T. K. Mondal and S. Mukhopadhyay, *Chem. Commun.*, 2013, **49**, 10739.

69. J. Wang, Y. Li, N. G. Patel, G. Zhang, D. Zhou and Y. Pang, *Chem. Commun.*, 2014, **50**, 12258.

70. M. Shellaiah, T. Simon, V. Srinivasadesikan, C. M. Lin, K. W. Sun, F. H. Ko, M. C. Lin and H. C. Lin, *J. Mater. Chem. C*, 2016, **4**, 2056.

71. S. Paul, A. Manna and S. Goswami, *Dalton Trans.*, 2015, **44**, 11805.

72. A. C. Goncalves, V. Pilla, E. Oliveira, S. M. Santos, J. L. Capelo, A. A. Dos Santos and C. Lodeiro, *Dalton Trans.*, 2016, **45**, 9513.